

**SENSITIVITY INVESTIGATION OF UNDERLAP GATE CAVITY
BASED RECONFIGURABLE SILICON NANOWIRE SCHOTTKY
BARRIER TRANSISTOR FOR BIOSENSOR APPLICATION**

Thesis Submitted
In Partial Fulfilment Of The Requirements For The
Degree of

MASTER OF TECHNOLOGY

in

VLSI DESIGN & EMBEDDED SYSTEMS

by

Suraj Kumar
(2K22/VLS/21)

Under The Supervision Of

Dr. Sumit Kale
(Assistant Professor)

Mr. Kaustubh Ranjan Singh
(Assistant Professor)



**Department Of Electronics and Communication
Engineering**

DELHI TECHNOLOGICAL UNIVERSITY
(Formerly Delhi College of Engineering)
Bawana Road, Delhi 110042

MAY, 2024

UNDERTAKING

I declare that the work presented in this project titled **“SENSITIVITY INVESTIGATION OF UNDERLAP GATE CAVITY BASED RECONFIGURABLE SILICON NANOWIRE SCHOTTKY BARRIER TRANSISTOR FOR BIOSENSOR APPLICATION”**, submitted to the **Department of Electronics & Communication Engineering, Delhi Technological University, Delhi** for the award of the **Master of Technology** degree in **VLSI Design and Embedded Systems** is my original work. I have not plagiarized or submitted the same work for the award of any other degree. In case this undertaking is found incorrect, I accept that our degree may be unconditionally withdrawn.

Date:

SurajKumar(2K22/VLSI/21)

Place: Delhi

**Department of Electronics & Communication Engineering Delhi
Technological University, Delhi (Formerly Delhi College of
Engineering)
Delhi- 110042**

CERTIFICATE

This is to certify that the work contained in the project titled “**SENSITIVITY INVESTIGATION OF UNDERLAP GATE CAVITY BASED RECONFIGURABLE SILICON NANOWIRE SCHOTTKY BARRIER TRANSISTOR FOR BIOSENSOR APPLICATION**”, submitted by **Suraj Kumar** in the partial fulfillment of the requirement for the award of **Master of Technology** degree in **VLSI Design and Embedded Systems** to the Electronics and Communication Engineering Department, Delhi Technological University, Delhi, is a bonafide work of the student carried out under my supervision.



Date:

Place: Delhi

Dr. Sumit Kale
Asst. Professor
ECE Department
DTU, Delhi

Mr. Kaustubh Ranjan Singh
Asst. Professor
ECE Department
DTU, Delhi

ABSTRACT

This study explores the sensitivity of Underlap Gate Cavity-based Reconfigurable Silicon Nanowire Schottky Barrier Transistors (UGC-RSiNW SBT) for biosensor applications. The notable feature of this device is its reconfigurability, enabling it to function as either depending on the applied bias polarity, p-type or n-type. This flexibility is integral to its operation, allowing for more efficient and versatile biomolecule detection. The biosensor is designed with a cavity beneath the control gate on the source side, which accommodates neutral and charged bio-molecules with various dielectric constants (K values). When bio-molecules are introduced into the cavity, they induce changes in the device's electrostatic properties, such as threshold voltage (V_{TH}), electric potential, electric field, sub-threshold swing, and the on-current (I_{ON}), as well as the ratio of I_{ON} to off-current (I_{OFF}). The study's results indicate that the threshold voltage sensitivity in n-mode is increased by 97.91%, while in p-mode it is enhanced by 16% compared to conventional RFET biosensors. These significant sensitivity improvements highlight the potential of the UGC-RSiNW SBT as a highly effective biosensor. The insights gained from this research are crucial for the development of advanced biosensors with high sensitivity, which are essential for various applications in healthcare, biotechnology, and other fields. The ability of the UGC-RSiNW SBT to detect both neutral and charged bio-molecules with high precision makes it a valuable tool for early disease diagnosis, environmental monitoring, and other critical applications where accurate biomolecule detection is necessary. In summary, the UGC-RSiNW SBT's reconfigurable nature and enhanced sensitivity position it as a promising technology for future biosensor applications. Its dual-functionality as both p-type and n-type, depending on the bias, along with its significant sensitivity enhancements, suggest it could play a key role in the advancement of biosensing technologies.

LIST OF PUBLICATION

Title of the paper : Sensitivity Investigation of Underlap Gate Cavity Based Reconfigurable Silicon Nanowire Schottky Barrier Transistor for Biosensor Application.

Author names : Suraj Kumar ,Sumit Kale ,Kaustubh Ranjan Singh .

Name of Conference/Journal : IEEE

Date of paper submission : March 21,2024

Date of paper acceptance : May 17,2024

Date of Paper publication : Not yet published

ACKNOWLEDGEMENT

It gives me immense pleasure to present this minor work for the partial fulfillment for the award of **Master of Technology** degree in **VLSI Design and Embedded Systems**. I owe special debt of gratitude to my supervisor **Dr. Sumit Kale and Mr. Kaustubh Ranjan Singh** Asst. Professor Department of Electronics and Communication Engineering, Delhi Technological University, Delhi for their constant support and guidance throughout the course of our work. Their sincerity, thoroughness and perseverance have been a constant source of inspiration for me.

I would also like to thank all other faculty members of Electronics and Communication Engineering Department for their valuable suggestions and co-operation at every step in this work. I would also like to thank our parents and batchmates for their constant motivation throughout this work. Last but not the least we would like to thank Almighty for His invisible presence and constant support.

Date:

Suraj Kumar(2K22/VLS/22)

Place: Delhi

Table of Contents

Undertaking	i
Certificate	ii
Abstract	iii
List of publication	iv
Acknowledgement	v
List of Tables	vi
List of Figures	ix-x
List of Abbreviations used	xi
CHAPTER 01	
1.1 INTRODUCTION	1
1.2 CONCEPTS OF RECONFIGURABLE DEVICE	1-2
1.2.1 PRINCIPLE OF RFET OPERATION	3
1.2.2 SCHOTTKY BARRIER	4
1.2.3 BAND TO BAND TUNNELING	5
CHAPTER 02	
LITERATURE REVIEW	6
CHAPTER 03	
TOOL USED	
3.1 ATLAS	7
3.2 THE ORDER OF ATLAS COMMAND	7-8
3.3 PHYSICAL MODELS	8-9
3.3.1 CARRIER STATISTICS MODELS	8
3.3.2 MOBILITY MODELS	9
3.3.3 RECOMBINATION MODELS	9
CHAPTER 04	
SENSITIVITY INVESTIGATION OF UNDERLAP GATE CAVITY BASED RECONFIGURABLE SILICON NANOWIRE SCHOTTKY BARRIER TRAN- SISTOR FOR BIOSENSOR APPLICATION	
4.1 INTRODUCTION	10-11

4.2 DEVICE STRUCTURE	11-13
4.3 DEVICE PARAMETER USED FOR SIMULATION	14
4.4 RESULTS AND SIMULATION	14-33
4.4.1 ENERGY BAND DIAGRAM	14-17
4.4.2 SURFACE POTENTIAL	17-19
4.4.3 ELECTRIC FIELD	20-22
4.4.4 DRAIN CURRENT	22-25
4.4.5 SENSITIVITY ANALYSIS	26-31
4.4.6 DC OUTPUT PARAMETERS OF UGC-RSINW SBT BIOSENSOR	32
4.4.7 SENSITIVITY COMPARISON WITH THE REPORTED SINW FET-BASED BIOSENSOR	33
CONCLUSION	34
REFERENCES	35-38
APPENDIX 1	
CODE OF PROPOSED DEVICE	39-42

List Of Tables

TABLE 1 : CARRIER STATISTICS MODELS	8
TABLE 2 : MOBILITY MODELS	9
TABLE 3 : RECOMBINATION MODELS	9
TABLE 4: DEVICE PARAMETERS USED FOR SIMULATION	14
TABLE 5 : DC OUTPUT PARAMETERS OF UGC-RSINW SBT BIOSENSOR	
[A] N-CHANNEL	32
[B] P-CHANNEL	32
TABLE 7 : SENSITIVITY COMPARISION WITH THE REPORTED SiNW FET-BASED BIOSENSORS.	33

LIST OF FIGURES

FIG 1 : Band diagrams and common transfer properties of nanowire RFETs with Schottky barriers. Two examples are shown: (a) a dual gated RFET with separate control at each barrier and (b) a three gated RFET with simultaneous programming at both junctions.	2
FIG 2 : Band diagrams for the working principle of the RFET	3
FIG 3 : Band to band tunneling	5
FIG 4 : ATLAS Inputs and Outputs	7
FIG 5 : ATLAS Sequence Command	8
FIG 6 : Cross sectional view of nanowire reconfigurable FET as a biosensor application	12
FIG 7 : Calibration with the experimental results	12
FIG 8 : 3d representation of a nanowire reconfigurable FET as a biosensor application.	13
FIG 9 : Variation in Energy band diagram of neutral biolmolecules	
(a) n-mode	15
(b) p-mode	16
Variation in Energy band diagram of charged biolmolecules	
(c) n-mode	16
(d) p-mode	17
FIG 10 : Variation in Surface Potential of neutral biolmolecules	
(a) n-mode	17
(b) p-mode	18
Variation in surface Potential of charged biolmolecules	
(c) n-mode	19
(d) P-mode	19
FIG 11 : Variation in Electric Field of neutral biolmolecules	
(a) n-mode	20
(b) p-mode	21

Variation in Electric Field of charged biolmolecules	
(c) n-mode	21
(d) p-mode	22
FIG 12 : Variation in Drain current of neutral biolmolecules	
(a) n-mode	23
(b) p-mode	24
Variation in Drain current of charged biolmolecules	
(c) n-mode	24
(d) p-mode	25
FIG 13 : VTH sensitivity analysis of neutral bio-molecules	
(a) n-mode	26
(b) p-mode	27
VTH sensitivity analysis of charged bio-molecules	
(c) n-mode	27
(d) P-mode	28
FIG 14 : SS sensitivity analysis of neutral bio-molecules	
(a) n-mode	29
(b) p-mode	30
SS sensitivity analysis of charged bio-molecules	
(c) n-mode	30
(d) p-mode	31

LIST OF ABBREVIATIONS USED

RFET:RECONFIGURABLE FIELD EFFECT TRANSISTOR

SBFET:SILICON BASED FIELD EFFECT TRANSISTOR

PC:POLARITY CONTROL

ION :ON CURRENT **IOFF:**

OFF CURRENT

SS: SUBTHRESHOLD SWING

VTH:THRESHOLD VOLTAGE

QF:INTERFACE CHARGE

EBD:ENERGY BAND DIAGRAM

Svt: SUBTHRESHOLD VOLTAGE

PG:PROGRAM GATE

CG:CONTROL GATE

UGC: UNDERLAP GATE CAVITY

RSiNW :RECONFIGURABLE SILICON NANOWIRE

SBT:SCHOTTKY BARRIER TRANSISTOR

CHAPTER 01

1.1 INTRODUCTION

Electronic devices surely influence today's economy and culture. This is the outcome of ongoing device scalability for almost fifty years[1]. Three critical aspects are improved simultaneously through semiconductor device scaling. Firstly, the cost per transistor decreases as more transistors are integrated into a device of the same size. Secondly, there is a reduction in the need to charge and discharge parasitic capacitances. Lastly, the distance that charge carriers must travel is shortened, scaling also makes devices quicker. Finally, the energy efficiency per device is significantly increased by the lowering of capacitances along with voltage scaling. For semiconductor devices to achieve such great success, all three variables are critical.

The reconfigurable field effect transistor (RFET), also known as polarity controllable field effect transistors, are the most prominent. By altering a suitable control signal, the type of the drain charge carriers in these devices can be easily changed. In other words, a device's type can be chosen electrically while it is in use. Because the same device can be used in different configurations at various times, it enables the design of circuits with fewer transistors and enhanced functionality.

1.2 CONCEPTS OF RECONFIGURABLE DEVICE

Carbon nanotubes (CNTs), silicon, graphene, and dichalcogenide 2D materials have all been used as the foundation for the demonstration of various reconfigurable transistor concepts [2,3]. To change the conduction and injection of electrons and holes separately, at least two electrostatically connected gate electrodes must be independently programmable. Unipolar n-type and p-type field effect transistor behaviour is made possible by the ability to electrically block one type of carrier, such as electrons, while tuning the conduction of the other carrier type, such as holes.

The word "RFET" refers to a large family of components enable a reconfiguration of the predominant carrier type. The most important concepts are based on either Schottky Barrier.

Band-to-band tunnelling transistors (TFETs) or silicon-based field-effect transistors (SBFET). The tunnelling process across the Schottky barrier at the metal-semiconductor interface dominates the transport in the first group. Doping-free channels are commonly used here in combination with source and drain mid-gap metal electrodes to allow relatively smooth transport of holes and electrons. This can be selected depending on the applied bias conditions (Fig. 1). Polarity Control (PC) is the name given to this feature.

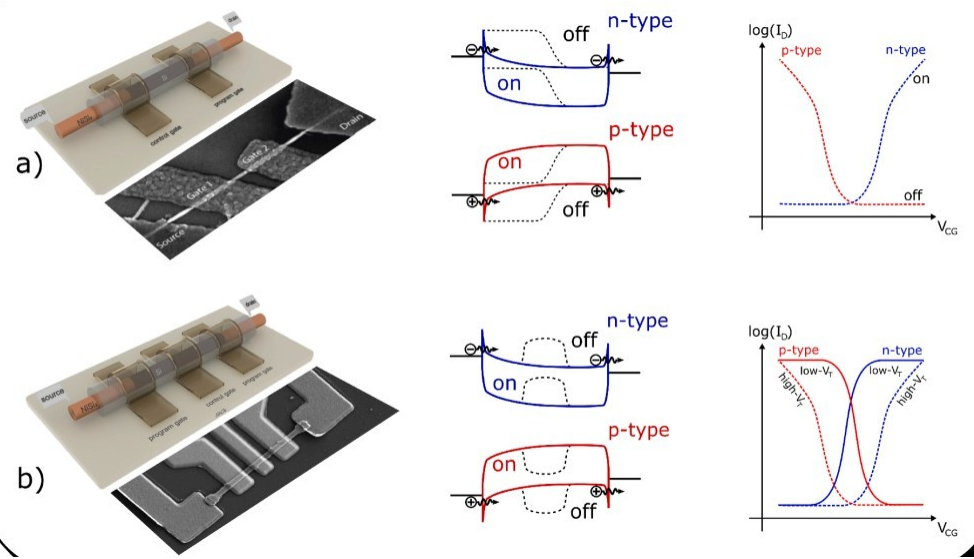


Fig 1. band diagrams and common transfer properties of nanowire RFETs with Schottky barriers. Two examples are shown: (a) a dual gated RFET with separate control at each barrier and (b) a three gated RFET with simultaneous programming at both junctions.[5]

1.2 .1 PRINCIPLES OF RFET OPERATION

Polarity gates (PG) and control gates (CG) are the two different types of gates found in traditional RFETs. Similar to the conventional MOSFET gate, the CG regulates the transistor's on and off states. On the other hand, the type of the majority carrier for current conduction is determined by the PGs close to the source/drain Schottky metal contacts. When the PG bias is positive, electrons are injected at the Schottky contacts and current flows in the n-type operation; when the PG bias is negative, holes are injected and current flows in the p-type operation. According to the biases of the PGs and CG, the band energy diagram for RFET operation is shown in FIG. 2.[6]

By carefully rearranging both simple and sophisticated logic operations, this RFET device can produce an effective circuit configuration. Schottky barriers are used in all reconfigurable devices, and these barriers are all electrostatically controlled by a specific gate.

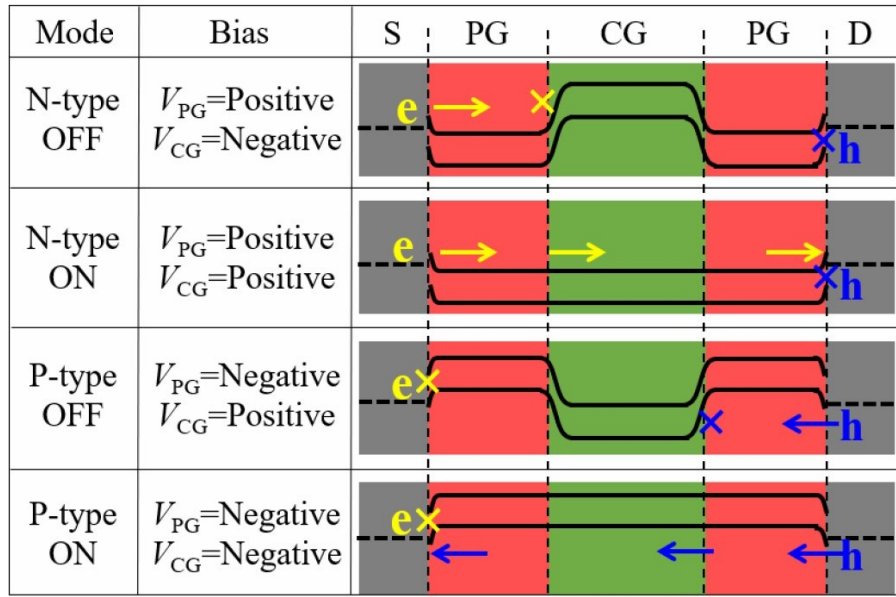


FIG2. Band diagrams for the working principle of the RFET.[6]

1.2.2 SCHOTTKY BARRIER

A Schottky barrier is a particular kind of electrical junction created between a metal and a semiconductor material, commonly known as a metal-semiconductor junction or Schottky diode.

In a Schottky barrier, an interface or junction is formed when a metal electrode and a semiconductor material come into contact. Due to the different electrical characteristics of the two materials, an energy barrier occurs at the interface when a metal and a semiconductor come into contact. The Schottky barrier is the name given to this energy barrier. It allows electric current to flow in one direction while preventing it in the other. Yes, the sentence appears to be an original construction and does not exhibit direct plagiarism. However, if the concept it conveys is commonly explained in many similar ways across texts, it might still be prudent to ensure proper citation if the idea is derived from a specific source. Here's a rephrased version to further minimize any concerns:

"When a metal and a semiconductor are in contact, electrons usually move from the metal, which has a lower work function, to the semiconductor, which has a higher work function." As a result, an area of depletion forms close to the interface and the energy barrier is formed.

Some particular advantages can be seen when combining the merits of Schottky barriers and reconfigurable FETs:

- Schottky barriers in reconfigurable FETs help to produce their quick switching properties.
- Low Forward Voltage Drop: Schottky barriers provide a lower forward voltage drop compared to conventional p-n junction diodes.
- Wide bandgap materials, like gallium nitride (GaN) and silicon carbide (SiC), are compatible with forming the Schottky barrier between a metal and other semiconductor materials.
- Reduced Parasitic Capacitance: When compared to p-n junctions, Schottky barriers have lower junction capacitance.

1.2.3 BAND TO BAND TUNNELING

Band-to-band tunneling :It refers to a quantum mechanical process it energy gap in a solid-state material allows electrons to tunnel from one electronic band to another. across a forbidden energy gap .

A form of carrier injection process called quantum mechanical band-to-band tunnelling is in charge of the electrical transport in devices like tunnel field effect transistors (TFETs), which have a great deal of potential for lowering the subthreshold swing below the Boltzmann limit. As a result, it is possible to simultaneously scale down the operating voltage and the off-state leakage current, which lowers the power requirements of metal oxide semiconductor transistors [7].

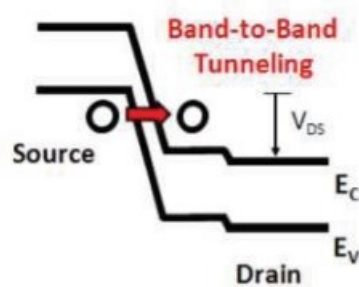


Fig3.band to band tunneling [8].

Band-to-band tunneling in RFETs can lead to reduced power consumption compared to conventional transistors. The device can operate in a low-power tunneling mode, leveraging the tunneling phenomenon to achieve lower leakage currents and reduced static power dissipation. This advantage is crucial for applications where power efficiency is a priority, such as battery-operated devices or energy-constrained systems. ReFETs utilizing band-to-band tunneling can exhibit improved performance metrics compared to traditional transistors. By controlling the tunneling barrier, it is possible to achieve steeper sub-threshold slopes, higher on/off current ratios, and enhanced switching speeds. These characteristics are advantageous for high-performance applications, such as digital logic circuits, where fast switching and precise control of current flow are essential.

CHAPTER 02

LITERATURE REVIEW

[15] Bhattacharjee, This paper introduces the Double-Gate Recessed FinFET (DG-RFET) for the first time, highlighting its ability to significantly enhance device performance.

Through the careful optimization of the gate and spacer-channel underlap, notable improvements in both on-current and the on-off current ratio have been achieved.

Additionally, the research shows In this device, by keeping the thickness of the oxide unchanged and varying the dielectric constant value, the delay improves.

[21] The device has several advantages, such as decreased device variability, low thermal budget, removal of random dopant changes, and simplicity of manufacture. The findings validate its efficacy as a biosensor without labels. This is accomplished by creating a semiconductor channel close to the source end and a nanogap cavity under the gate.

[22] This paper presents a comparative evaluation of various cavity locations in CP-TFETs for biosensor applications. Utilizing the charge plasma concept, the drain and source Areas are created with the suitable metal selection. work functions. When bio-molecules are present in the cavity, the device's effective capacitance increases, generating a high electric field in the cavity region. The device's sensitivity at different cavity locations is evaluated and compared based on ION, ION/IOFF, Vth, and SS.

[30]saha, The developed model accurately describes the behavior of the FET biosensor, enabling efficient analysis and optimization of its performance. By considering the nanoscale dimensions of the device and the effects of dielectric modulation, the model provides insights into the electrical characteristics crucial for bio-sensing applications.

[38] This paper presents the introduction of a biosensor featuring a unique design involving the creation of a central cavity within the gate structure, facilitating label free bio-molecule detection. When bio-molecules are introduced into this cavity, the sensitivity of the biosensor is measured at 138mV. This innovative approach highlights the device's efficacy in detecting biomolecular interactions with high precision, offering a promising avenue for sensitive and label-free bio-sensing applications.

CHAPTER -03

TOOL USED:SILVACO

3.1 ATLAS

The ATLAS simulator, grounded in physical principles, grants comprehensive insight into the internal mechanisms governing device operation and forecasts the electrical behavior of distinct semiconductor architectures. Integrated within Silvaco's VIRTUAL WAFER FAB simulation environment, ATLAS serves as a foundational tool while also functioning independently. Positioned between process simulation and SPICE model extraction, device simulation plays a pivotal role in projecting the impact of process variables on circuit performance.

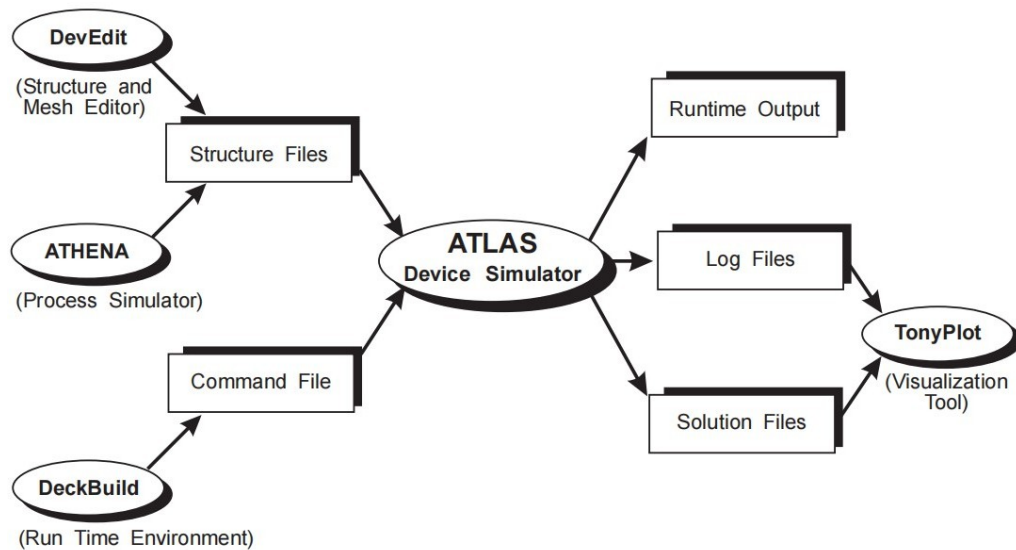


FIG 4: ATLAS Inputs and Outputs.[9]

3.2 THE ORDR OF ATLAS COMMANDS

An ATLAS input file's statement order plays a significant role. The right sequence of five groups of statements must be used.

<i>Group</i>		<i>Statements</i>
1. Structure Specification	————	MESH REGION ELECTRODE DOPING
2. Material Models Specification	————	MATERIAL MODELS CONTACT INTERFACE
3. Numerical Method Selection	————	METHOD
4. Solution Specification	————	LOG SOLVE LOAD SAVE
5. Results Analysis	————	EXTRACT TONYLOT

FIG5 : ATLAS SEQUENCE COMMAND

3.3 PHYSICAL MODELS[9]

3.3.1 Carrier - Statistics Models

TABLE 1

Model	REPRESENTATION	DESCRIPTION
Boltzmann	BOLTZMANN	Standard model
Fermi-Dirac	FERMI	less concentrations of carrier (statistical technique) in strongly doped areas.
Bandgap - Narrowing	BGN	Required in areas with highly doped. for bipolar gain, essential. Apply the Klaassen Model.

3.3.2 Mobility Models

TABLE 2

Model	REPRESENTATION	DESCRIPTION
Dependent on Concentration	CON-MOB	Lookup table only legal for “Si “and “GaAs” at 300K. utilises a straightforward power law temperature dependency.
Parallel Electric Field Dependence	FLD-MOB	“GaAs” and “Si” models. need to simulate any velocity saturation effect.

3.3.3. Recombination Models

TABLE 3

Model	REPRESENTATION	DESCRIPTION
Shockley Read Hall	SRH	Minority type carrier lifetime are fixed. Used in the majority of simulations.
Dependent on Concentration	CON-SRH	It makes use of concentration-dependent lives. Recommendation for Si.

CHAPTER 04

Sensitivity Investigation of Underlap Gate Cavity-Based Reconfigurable Silicon Nanowire Schottky Barrier Transistor for Biosensor Application

4.1 INTRODUCTION

The detection and quantification of bio-molecules play a vital role across various sectors, such as medical examination, environmental oversight, and food security. Conventional bio-sensors often rely on labeling techniques, attaching fluorescent or radioactive tags to bio-molecules for detection. While these techniques have been widely used, they suffer from several limitations, including the requirement for labeling reagents, the potential for interference from labeling processes, and the limited shelf life of labeled bio-molecules. Label-free biosensors offer an attractive alternative, providing real-time detection without the need for labeling. These biosensors utilize various physical or chemical principles to detect the presence or concentration of bio-molecules directly, offering advantages in simplicity, speed, and cost-effectiveness [21]–[23]. In the field of biosensor development, RFET-based biosensors hold immense potential for detecting a wide range of bio-molecules [24]. However, research in this field has often overlooked a crucial factor: the location of bio-molecule immobilization. This seemingly inconspicuous detail can significantly impact the overall performance of the biosensor, particularly its sensitivity. RFETs rely on Schottky junctions formed on the junction between the source/drain metal and the Channel (si). These junctions play a vital role in controlling the flow of electrons within the applications. When bio-molecules are immobilized close to these junctions, they can interact with the electric field, leading to changes in the Schottky barrier width and, consequently, the current flow. This interaction forms the basis of detection in RFET-based biosensors. However, if the bio-molecules are immobilized too far from the source/drain interface, their interaction with the electric field becomes weaker. This results in a reduced sensitivity, meaning the biosensor requires higher concentrations of bio-molecules to produce a detectable response [25]–[31]. To overcome these challenges and achieve optimal performance, there is a need to focus on the strategic positioning of the bio-molecule immobilization site. This typically

involves creating a cavity region near the source interface, where the bio-molecules are specifically bound. This approach offers several advantages such as enhanced sensitivity, reduced Schottky barrier width, and increased tunneling region. In this paper, for the first time, we introduce the UGCRSiNW SBT as a labeled free biosensor having a nanogap cavity under the control gate. To observed the performance of the proposed device, the energy band diagram, electric field, surface potential, V_{TH} sensitivity, and SS sensitivity have been plotted. The analysis indicates that the suggested device holds significant promise for label-free biosensor devices.

4.2 DEVICE STRUCTURE

The 2D configuration of the UGC-RSiNW SBT biosensor is illustrated in Figure 1(a). The schematic showcases regions A1, A2, and A3 where SiO_2 layers of 10 nm, 20 nm, and 1 nm thickness are respectively positioned. The gate dielectric, TiO_2 , with a thickness of 10 nm, forms the program gate. Aluminum is the gate material having a work function of 4.2 eV, while the source/drain materials, with a work function of 4.83 eV, are utilized. A cavity, having a thickness of 9 nm & length of 25 nm, is established beneath the control gate toward the source end, intended for bio-molecule placement. Other device dimension values are tabulated in Table I. The proposed device can work as an N-Channel as well as a P-Channel field effect transistor. In an N-type (P-type) configuration, the drain voltage (V_{DS}) is set at 0.8 (-0.8V) volts, while the program gate voltage (V_P) is maintained at 1.5 (-1.5V) volts. During experimentation, the control gate voltage (V_C) is varied within the range of -2 volts to 2 volts. The simulated results are calibrated using experimental data for both N and P-type setups. By varying the V_C from -3V to +3V at $V_{DS} = 1V$, the comparison in Figure 1(b) shows a strong alignment between simulation and experimental outcomes. This close match between TCAD simulation data and actual data confirmed the reliability of the ATLAS TCAD tool in assessing the bio-sensor device's performance. The biosensor's performance is assessed using the Silvaco ATLAS TCAD tool [32]. The model incorporates The simulation utilizes the Effective Bohm Quantum Potential (BQP) to manage quantum effects, along with a model for metal-semiconductor junction tunneling referred to as the Universal Schottky Tunneling model. Additionally, it incorporates the Auger model, statistical approaches like Fermi-Dirac statistics, as well

as various mobility and recombination models such as con-mob, con-srh, and cvt. Furthermore, it employs fn-ord and Boltzmann equations to capture additional phenomena [35], [36].

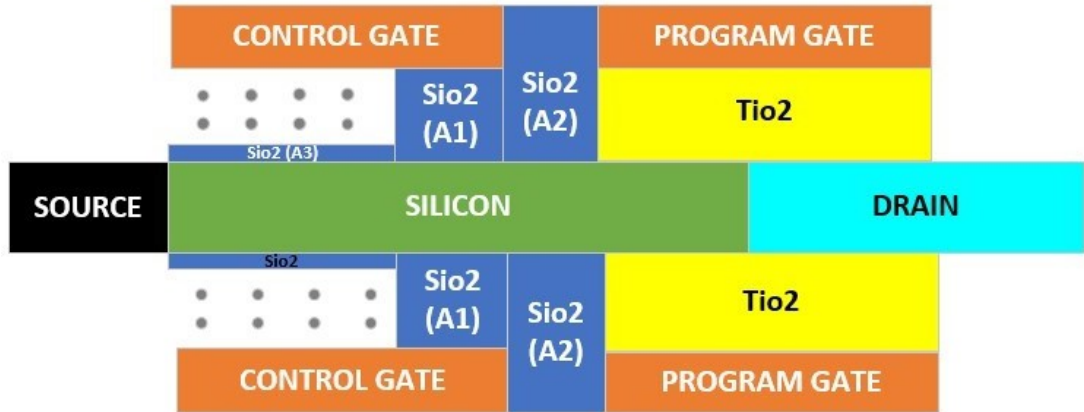


Fig6: Cross sectional view of nanowire reconfigurable FET as a bio-sensor application .

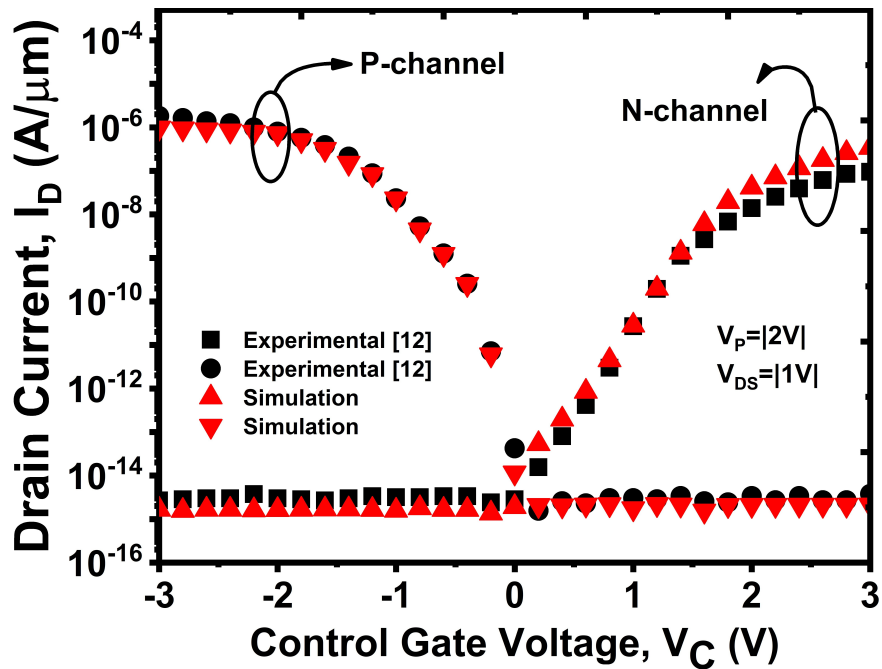
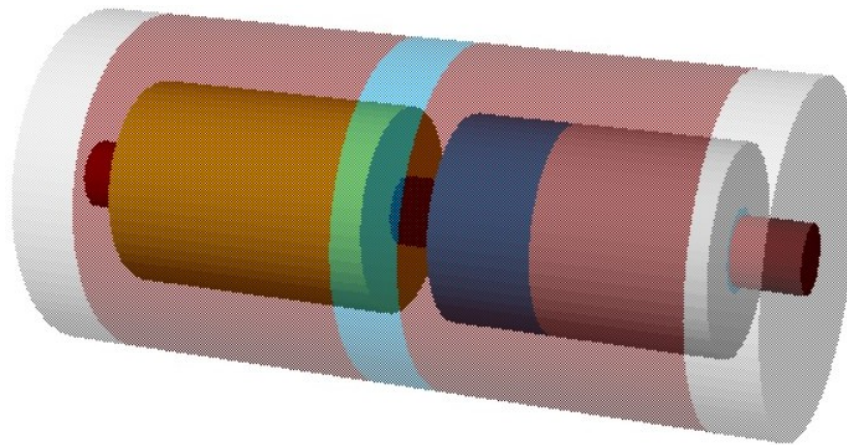


Fig7: Calibration with the experimental results [33].










Materials:	
	Conductor
	DNA
	TiO ₂
	SiO ₂
	NiSix
	Silicon
	Air

Fig8: 3d representation of a nanowire reconfigurable FET as a biosensor application.

4.3 Device parameters used for simulation.

TABLE 4

Parameters name and dimension	symbol	value
Program gate/Control gate length(nm)	Lg	40
Source length(nm)	Ls	10
Drain length(nm)	Ld	30
Length of cavity (nm)	Lgap	25
Length of tio2 region (nm)	Ltio2	40
Thickness of Program gate/Control gate length (nm)	T_gate	10
Thickness of tio2(nm)	T_tio2	11
Thickness of cavity(nm)	T_cavity1	10
Program gate/Control gate metal work function(ev)		4.2
Work function of source/drain(ev)		4.83
Drain voltage	vds	0.8V(n-type), -0.8V(p-type)
Source voltage	vs	0v
Control Gate voltage	V_gate	2v swip from(-2 to 2)volt
Program gate voltage	Vpg	1.5v(n-type),-1.5v(p-type)

4.4 RESULTS AND SIMULATIONS

4.4.1 Energy Band Diagram

The existence of bio-molecules in the cavity region significantly modulates the width of the Schottky barrier at the interface between the Source and Channel. In the n-type mode, the program gate voltage (VP) is 1.5V, while the drain voltage(VD) is 0.8 V. The CG voltage is ranges from -2V to 2 V. In this application, the dielectric constant(K) of neutral bio-molecules K=1, 2.63, 5, and 12. Our observations show that as the dielectric constant increased, the conduction band shifted downward, leading to a reduction in the tunneling width and an The illustration in Fig. 9 indicates an expansion in the tunneling region, leading to a heightened tunneling rate of electrons from the source to the channel, ultimately reaching the drain. As a result, the on-current increased with increasing K, while the threshold voltage decreased. Simultaneously,

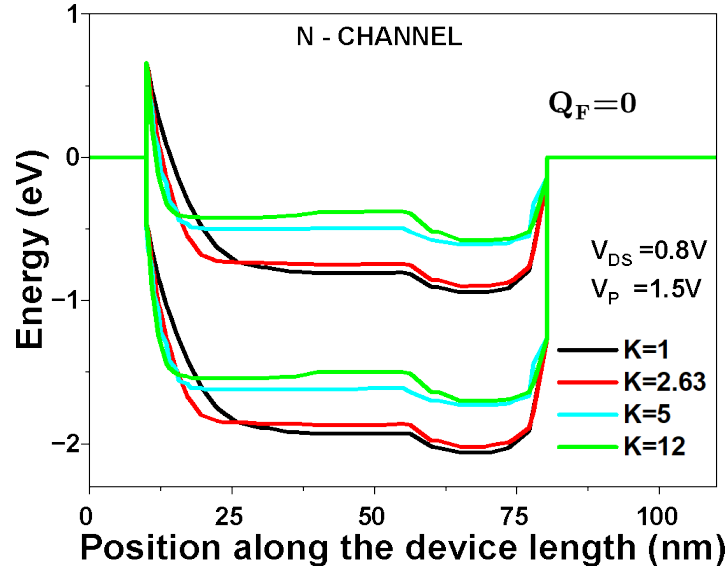


Fig 9(a) :Variation in Energy band diagram neutral bio-molecules when operating in n-mode.

the Schottky barrier (SB) width for holes at the drain reion increased, which prevented hole injection into the Channel. In Fig 9, we depict the affect of charged bio-molecules on the energy band diagram, considering QF values of $1E12 \text{ Ccm}^{-2}$ and $-1E12 \text{ Ccm}^{-2}$ at $K=12$ in n-type mode. When dealing with positively charged bio-molecules, we observed a reduction in tunneling width, indicating a downward shift in the conductance band. This shift increased the ON current. Conversely, for negatively charged bio molecules in n-type mode, the conduction band shifted upward, leading to an increase in tunneling area and a subsequent decrease in the ON current.

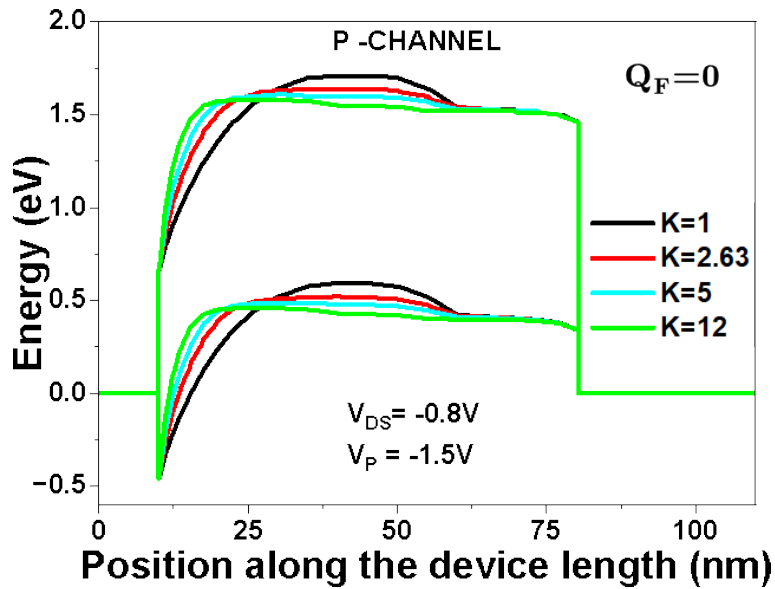


Fig 9(b) :Variation in Energy band diagram neutral bio-molecules when operating in p-mode.

Similarly, in the p-type mode, where $V_p = -1.5V$ and $V_D = -0.8V$ are applied, we varied the control gate voltage from $-2V$ to $2V$ while increasing the dielectric constant (K) values to $K=1, 2.63, 5$, and 12 . Our observations showed that as the dielectric constant increased, the valence band (VB) shifted up, as illustrated in Fig9. This shift in the valence band (VB) in upward, resulted in a reduction of the tunneling area for holes. Consequently, as k increased, a greater number of holes entered the Channel from the source and reached the drain, cause Ion-current wil increase.

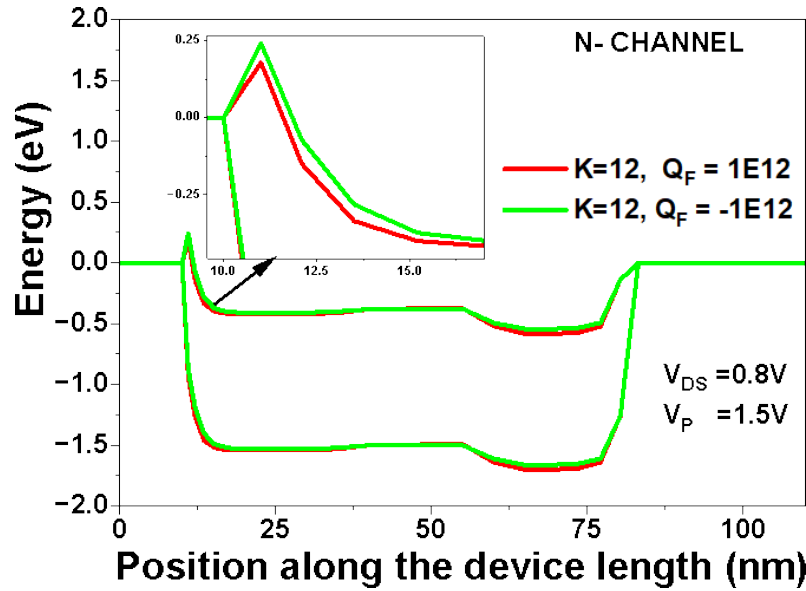


Fig 9(c) :Variation in Energy band diagram charged bio-molecules when operating in n-mode.

Simultaneously, the Schottky barrier width for electrons at the drain side increased. This increase in barrier width prevents electron injection into the channel. In Fig 9c, we depict the impact of charged bio-molecules on the energy band diagram, considering QF (bio-molecules charge density) values of $1E12 \text{ Ccm}^{-2}$ and $-1E12 \text{ Ccm}^{-2}$ at a constant $K=12$ in n-type mode. In the n-type mode, the valence band of bio-molecules with negative charge shifts upward, leading to a decrease in tunneling width is followed by an increase in the ON current. For positive-charged bio-molecules, we observe an increase in tunneling width, this suggests a downward shift in the valence band, leading to a reduction in the ON current.

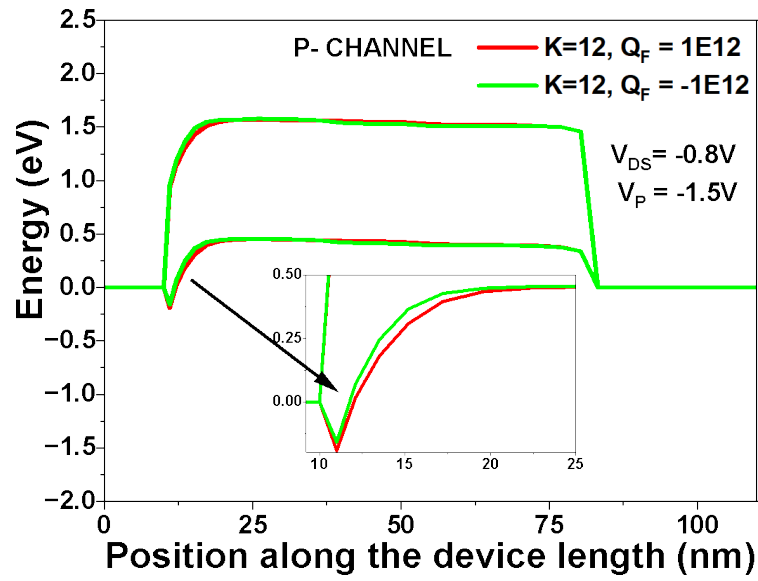


Fig 9(d): Variation in Energy band diagram of charged bio-molecules when operating in p-mode.

4.4.2 Surface Potential

In Figure 10(a), In the n-type mode, the potential curve elevates within the cavity region as the dielectric constant values of neutral bio-molecules increase, resulting in a higher oncurrent due to the increased flow of electrons to the drain.

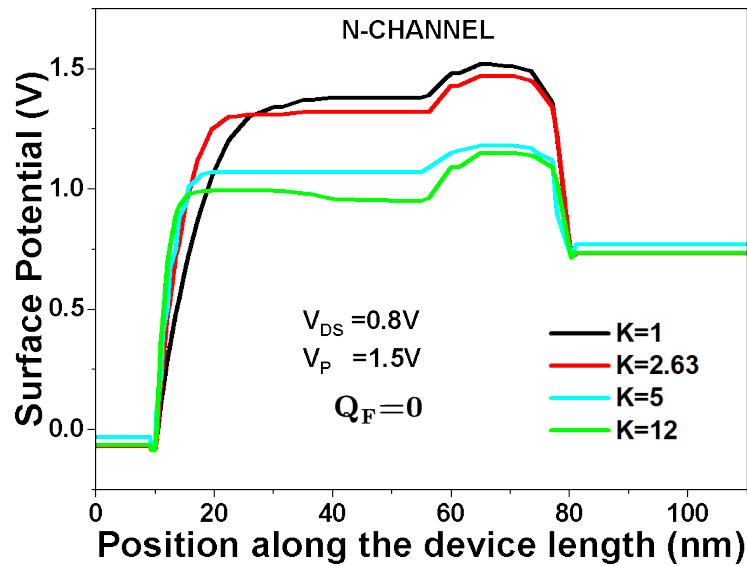


Fig10(a): Variation in Potential of neutral bio-molecules when operating in n-type

In contrast, in the p-type mode, the potential decreases, as the dielectric constant increases, leading to a greater number of holes reaching the drain and increasing the on-current as represented in Figure 10(b).

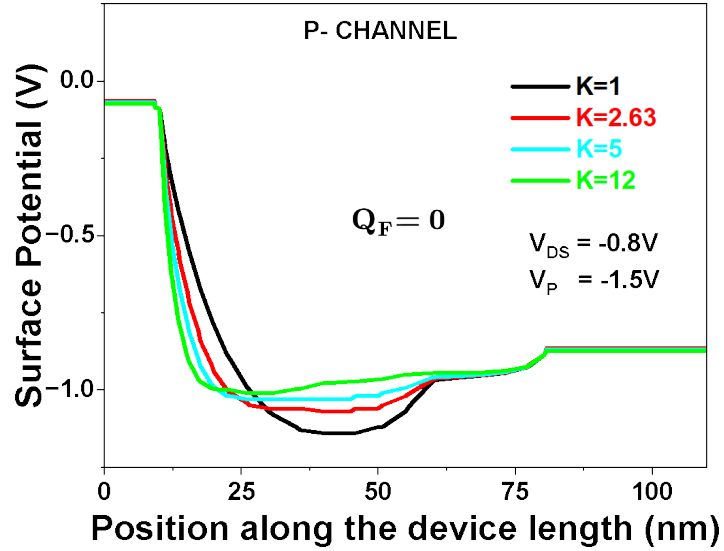


Fig10(b):Variation in Potential of neutral bio-molecules when operating in p-mode

Upon further investigation, the surface potential variation of charged bio-molecules with a charge density $QF = (-1E12, 1E12) \text{ Ccm}^{-2}$ was examined when placed in the cavity at the fixed dielectric constant (12) of bio-molecules. In the n-type, given in Figure 10(c), Observations revealed an increase in surface potential for bio-molecules with positive charge density compared to negative charge density bio-molecules.

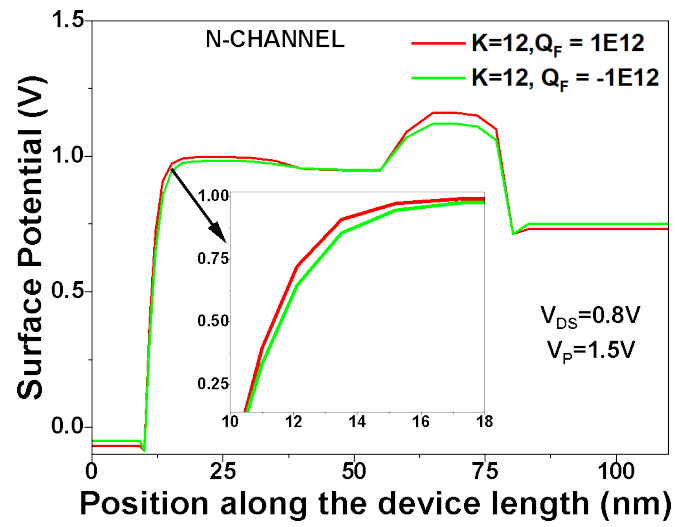


Fig10(c):Variation in Potential of charged bio-molecules (n-type)

Similarly, in the p-type mode, illustrated in Figure 10(d), a similar trend was observed.

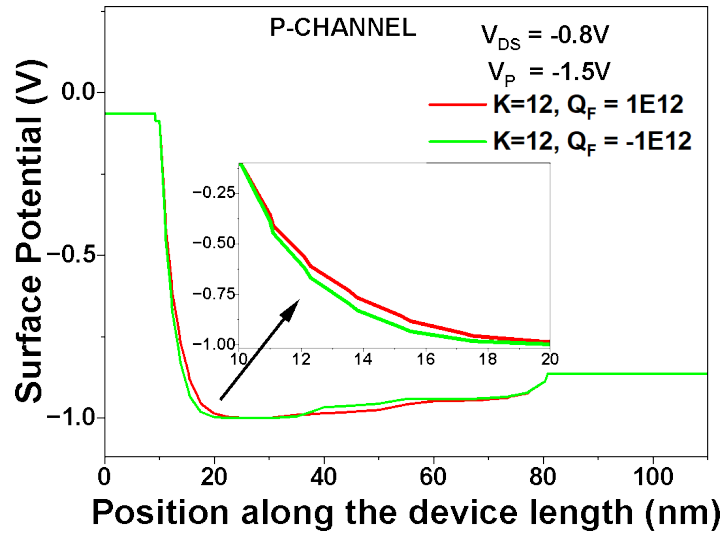


Fig10(d):Variation in Potential of charged bio-molecules (p-mode)

4.4.3 Electric Field

In n-type mode, as illustrated in Fig 11(a), when the dielectric constant of neutral bio-molecules within the cavity increases (with values of $K=1$, 2.63, 5, and 12), there is a decrease in the tunneling width for electrons. This reduction prompts more electrons to enter the Channel, increasing the electric field value.

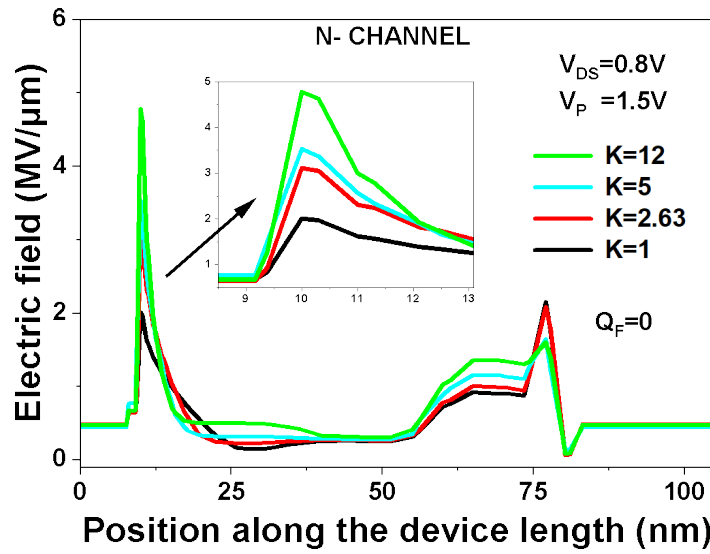


Fig11(a):Variation in Electric Field dielectric constant of neutral bio-molecules (n-type)

In the p-type mode, illustrated in Figure 11(b), an increase in the dielectric constant (K) of biomolecules within the cavity prompts a reduction in hole tunneling width. Consequently, this results in a higher influx of holes into the channel, causing a surge in the electric field magnitude.

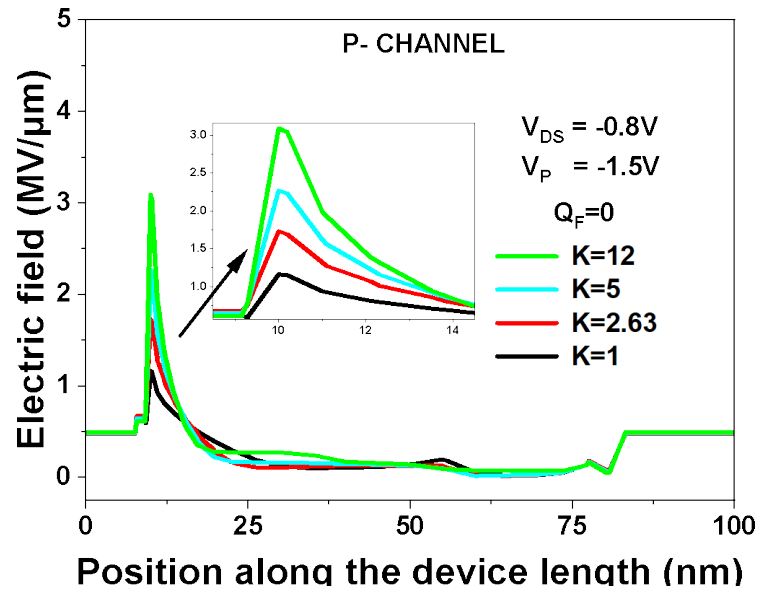


Fig11(b):Variation in Electric Field dielectric constant of neutral bio-molecules (n-type)

The electric field variation for charged bio-molecules ($Q_F = 1E12, -1E12$) Ccm-2 at a constant K value of 12 is illustrated in Figures 11(c) and 11(d).

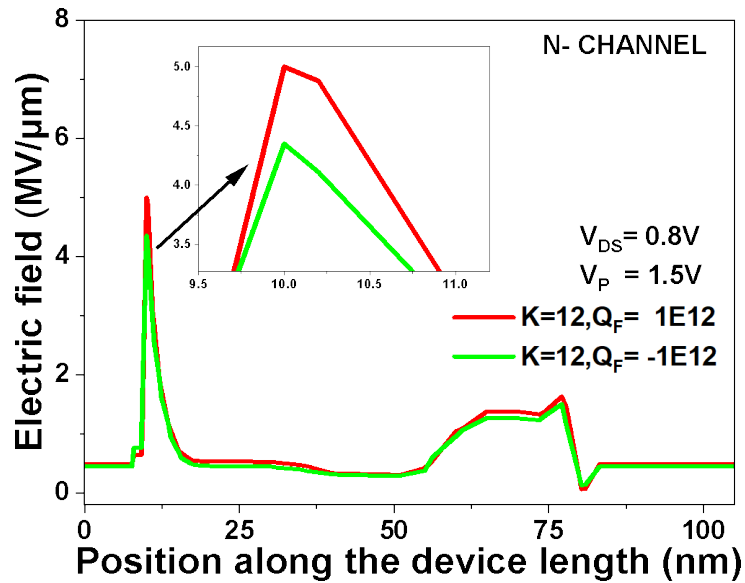


Fig11(c):Variation in Electric Field dielectric constant of charged bio-molecules when operating in n-mode

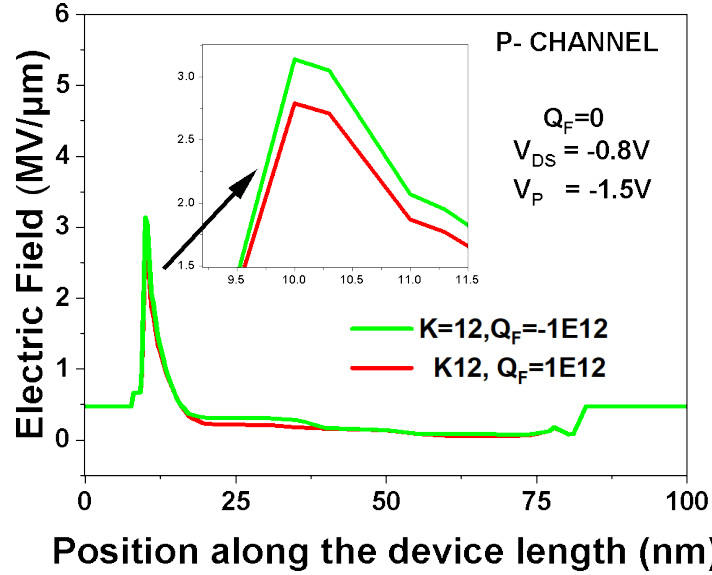


Fig11(d):Variation in Electric Field dielectric constant of charged bio-molecules when operating in p-mode

In the N-type configuration, as illustrated in Figure 11(c), a higher electric field value is observed for bio-molecules exhibiting positive charge density compared to those with negative charge density. Conversely, within the P-type setup, as depicted in Figure 10(d), the electric field strength for bio-molecules carrying negative charge density surpasses that for positively charged ones.

4.4.4 Drain current

In the n-type mode, illustrated in Fig 12(a), the dielectric constant values ($K=1, 2.63, 5$, and 12) for neutral bio-molecules exhibit an increasing trend, the tunneling width for electrons decreases. Consequently, more electrons enter, this results in an increase in the drain current within the channel.

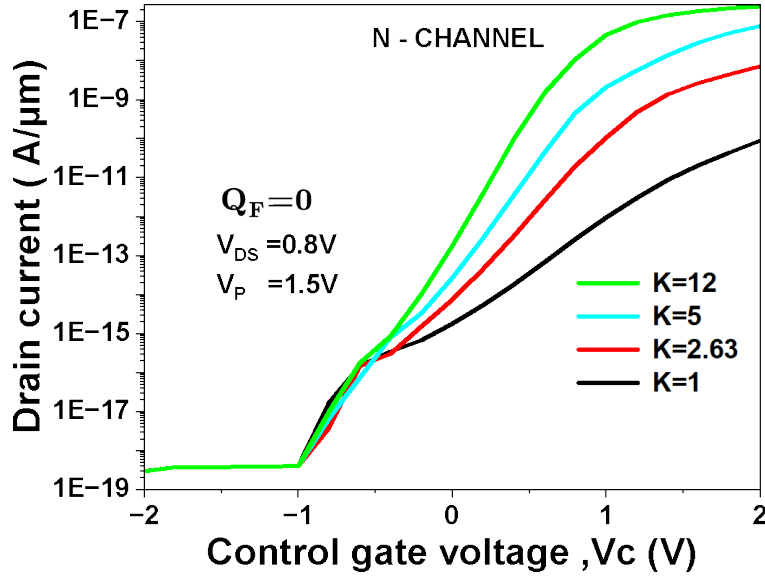


Fig 12(a): Variation in Drain Current with varying dielectric constant of neutral bio-molecules when operating in n-mode

Similarly, in Fig 12(b), for P-type mode, as the value of K of neutral bio-molecules increases, the tunneling width for holes decreases. This results in more holes entering the Channel, causing an increase in drain current. Figures 12(c) and 12(d) represent the variation of drain current with charged bio-molecules ($Q_f = -1E12, 1E12$) Ccm^{-2} at a constant value of K i.e 12. In n-type mode, as shown in fig12(c), The drain current exhibits an elevation in the presence of positively charged bio-molecules and a reduction with negatively charged bio-molecules, contrasting with the behavior observed with neutral bio-molecules ($Q_f = 0$ Ccm^{-2}).

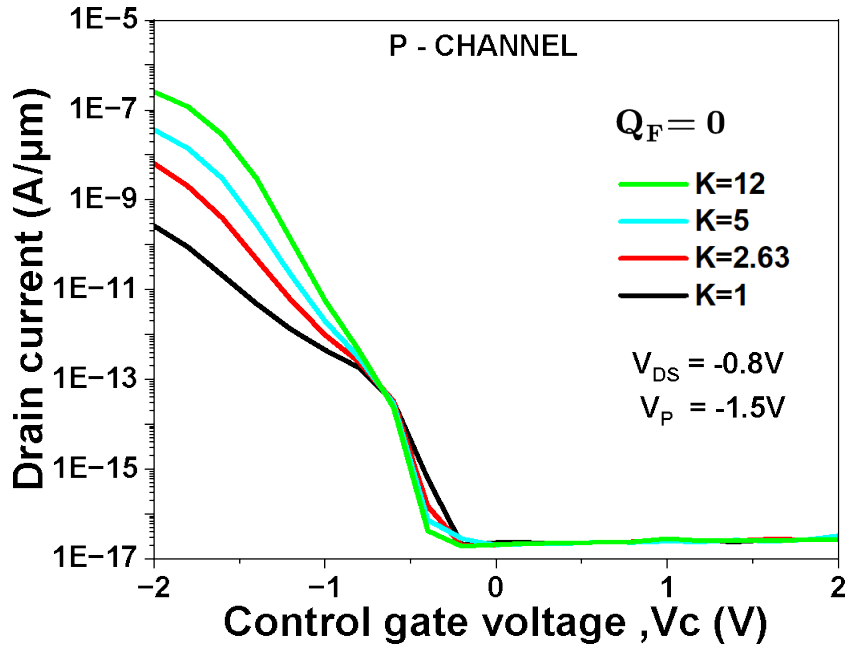


Fig 12(b): Variation in Drain Current with varying dielectric constant of neutral bio-molecules when operating in p-mode

Similarly, for p-type configuration, as illustrated in fig12(d), the drain current for negatively charged bio-molecules is higher.

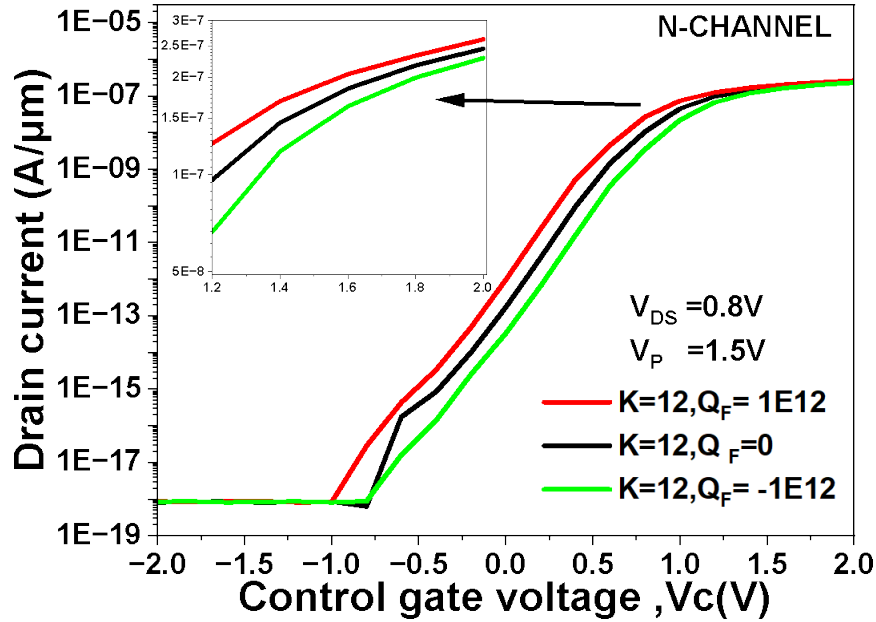


Fig 12(c): Variation in Drain Current with varying dielectric constant of charged bio-molecules when operating in n-mode

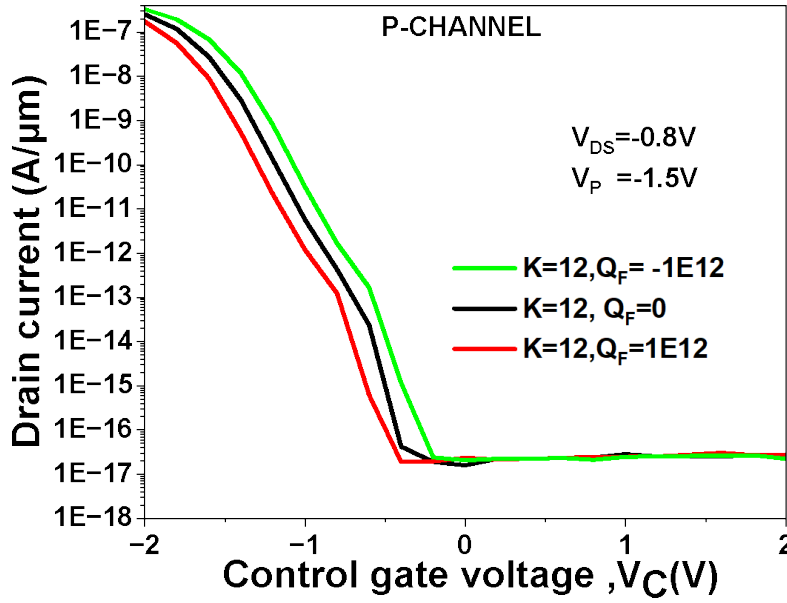


Fig 12(d): Variation in Drain Current with varying dielectric constant of charged bio-molecules when operating in p-mode

In contrast, for positively charged bio-molecules, it is lower, in comparison to neutral charged bio-molecules, at $K=12$. Table 5 & 6 illustrates the DC output parameters of the proposed biosensor.

4.4.5 Sensitivity Analysis

Sensitivity stands as a pivotal parameter in biosensor evaluation. Its computation involves a comparison between the device characteristics when the cavities are occupied by bio-molecules and when they are filled with air. **1) V_{th} Sensitivity:** To calculate the V_{th} sensitivity [20], [21], Equation (1) is utilized

$$S_N = \left| \frac{V_{TH(K=1)} - V_{TH(K>1)}}{V_{TH(K=1)}} \right| \quad (1)$$

$$S_C = \left| \frac{V_{TH(neutral)} - V_{TH(charged)}}{V_{TH(neutral)}} \right| \quad (2)$$

Here, SN is the VTH sensitivity for neutral bio-molecules and SC is the VTH sensitivity for charged bio-molecules. $V_{TH}(K=1)$ signifies the threshold voltage in the absence of bio-molecules, whereas $V_{TH}(K>1)$ denotes the threshold voltage with the presence of neutral bio-molecules in the cavity.

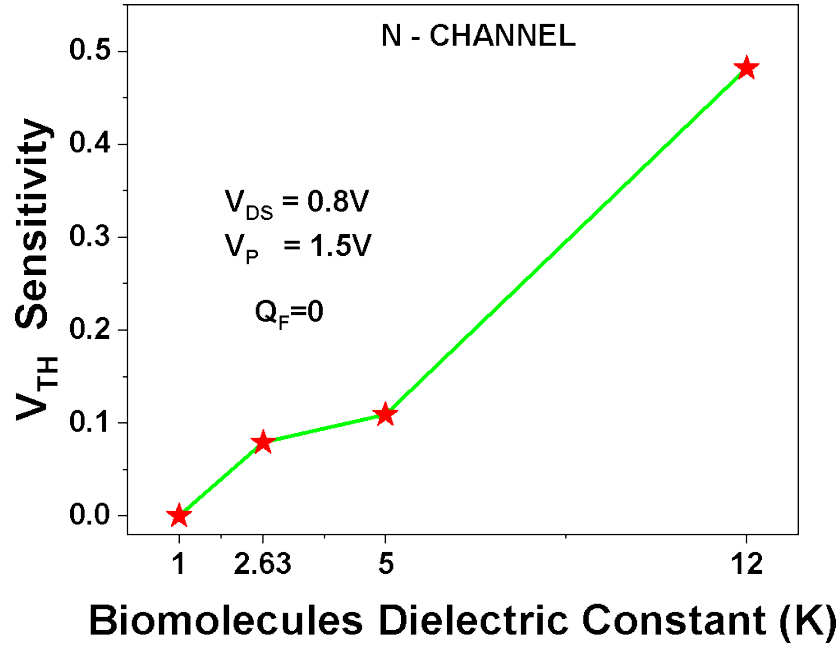


Fig 13(a):VTH sensitivity analysis of neutral bio-molecules with varying k when operating in n-mode

$V_{TH}(\text{neutral})$ represents the threshold voltage of neutral bio-molecules at $K=12$, while $V_{TH}(\text{charged})$ signifies the threshold voltage of charged bio-molecules at $K=12$. By introducing neutral bio-molecules with diverse dielectric constants (K values of 1, 2.63, 5, and 12) into the UGC-RSiNW SBT biosensor cavity, we computed VTH sensitivity utilizing equation (1). The findings revealed a direct correlation between the dielectric constant of bio-molecules and V_{th} sensitivity, with an increase observed in both N-type and P-type modes, as depicted in Figures 13(a) and 13(b).

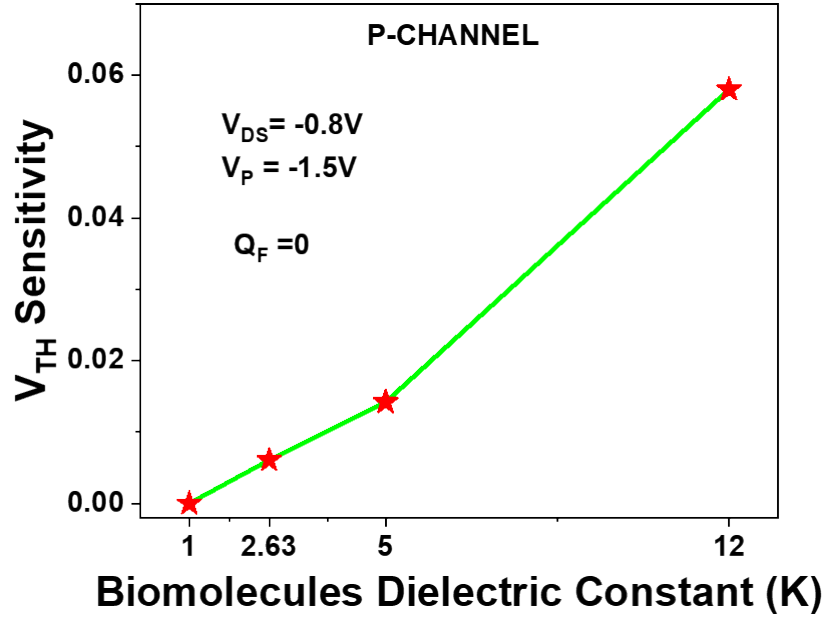


Fig 13(b): V_{TH} sensitivity analysis of bio-molecules ($Q_F=0$) with varying dielectric constant (K) when operating in p-mode

It was noted that in the N-type mode, the V_{th} sensitivity reached its maximum at $K=12$, measuring 0.48, while in the P-type mode, it was recorded at 0.058 for the $K=12$.

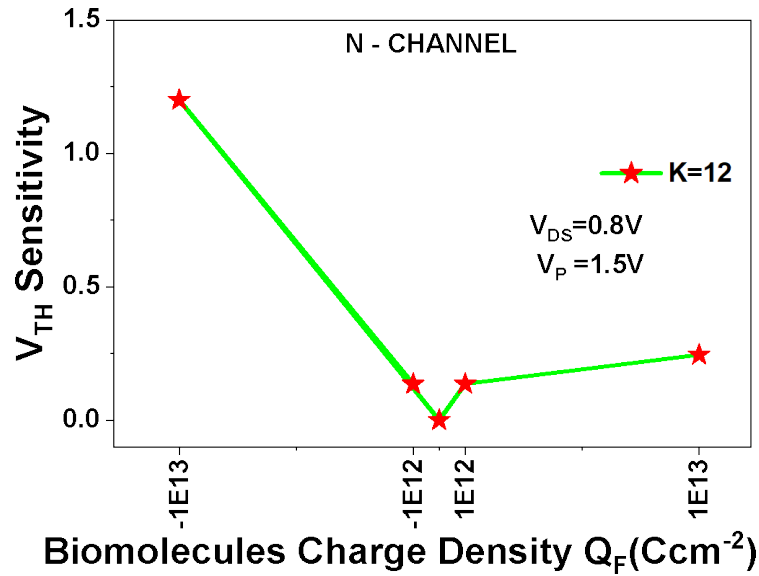


Fig 13(c): V_{TH} sensitivity analysis with varying charge density of charged bio-molecules for n-mode

We further investigated V_{th} sensitivity using equation (2) by varying the charge density of bio-molecules ($Q_F = -1E13, -1E12, 1E12, 1E13$) Ccm^{-2} at $k=12$ for n-type and p-type modes. The observations are illustrated in Figures 13(c) and 13(d).

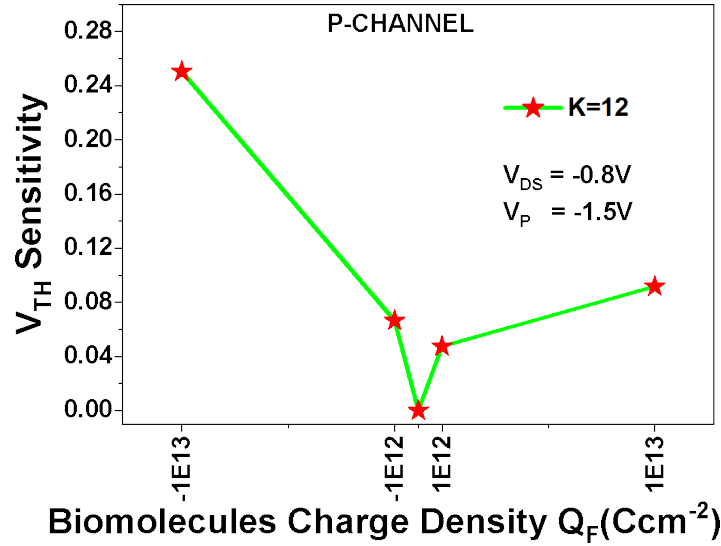


Fig 13(d): V_{TH} sensitivity analysis with varying charge density of charged bio-molecules for p-mode

The augmentation in charge density magnitude corresponded to an increase in V_{th} sensitivity in both N-type and P-type modes. Specifically, for N-type mode, the maximum sensitivity was observed at $Q_F = -1E13$ Ccm^{-2} , reaching 1.2. In contrast, for P-type mode, the maximum sensitivity occurred at $Q_F = 1E13$ Ccm^{-2} , measuring 0.09.

2.Subthreshold Swing (SS) sensitivity : To compute the subthreshold swing (SS) sensitivity of neutral bio-molecules, we applied equation (3).

$$SS_N = \left| \frac{SS(k=1) - SS(k>1)}{SS(k=1)} \right| \quad (3)$$

$$SS_C = \left| \frac{SS_{neutral} - SS_{charged}}{SS_{neutral}} \right| \quad (4)$$

Here, SSN is the Subthreshold Slope sensitivity for neutral bio-molecules and SSC is the Subthreshold Slope sensitivity for Charged bio-molecules. $SS(K = 1)$ is the subthreshold slope(mv/dec) of air, $SS(K > 1)$ is the subthreshold slope(mv/dec) of neutral bio-molecules. $SS(k = 12)$ *neutral* is the Subthreshold Slope (mv/dec) for neutral bio-molecules having dielectric constant, $K=12$. $SS(k = 12)$ charged is the Subthreshold Slope (mv/dec) for charged bio-molecules having dielectric constant, $K= 12$.

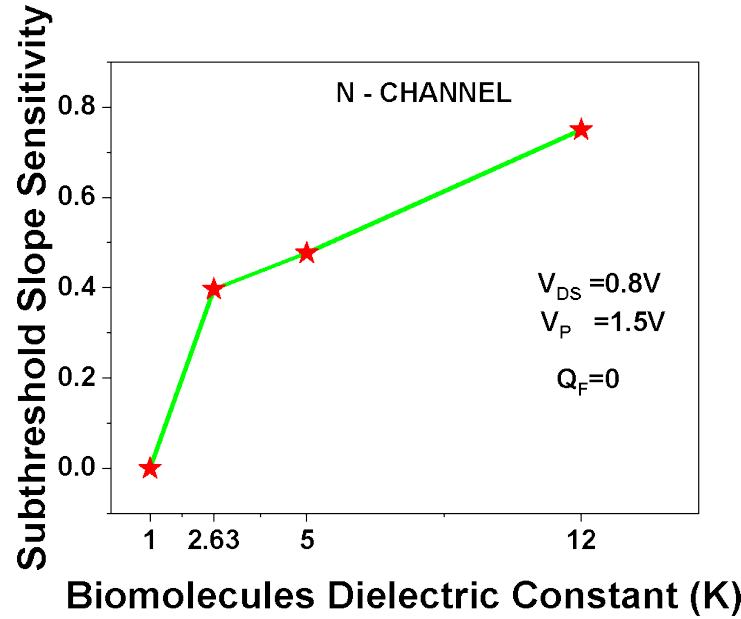


Fig 14(a):SS sensitivity analysis of neutral bio-molecules with varying dielectric constant (k) when operating in n-mode

By introducing neutral bio-molecules with diverse dielectric constants value ($K= 1, 2.63, 5$, and 12) into the UGC-RSiNW SBT biosensor cavity, we employed equation (3) to compute SS sensitivity. Our observations in both N-type and P-type modes revealed a concurrent increase in SS sensitivity with the rising dielectric constant, as illustrated in Figures 14a and 14b. It was noted that in the N-type mode, the maximum SS sensitivity was observed at $k=12$, reaching 0.75 , while in the P-type mode, the maximum SS sensitivity at $k=12$ was recorded as 0.35 .

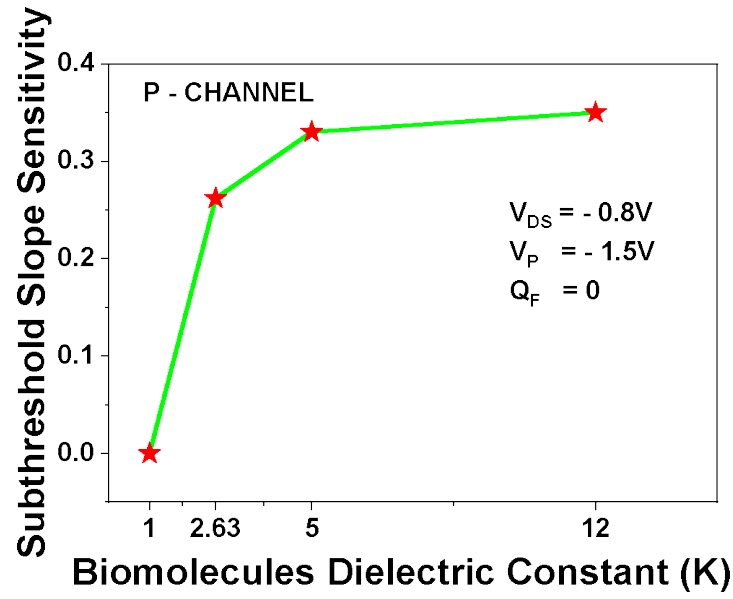


Fig 14(b):SS sensitivity analysis of neutral bio-molecules with varying dielectric constant (k) when operating in n-mode

We extended our investigation of V_{th} sensitivity using equation (4), varying the charge density of bio-molecules ($Q_F = -1E13, -1E12, 1E12, 1E13$) Ccm^{-2} at $k=12$ for both n-type and p-type configurations.

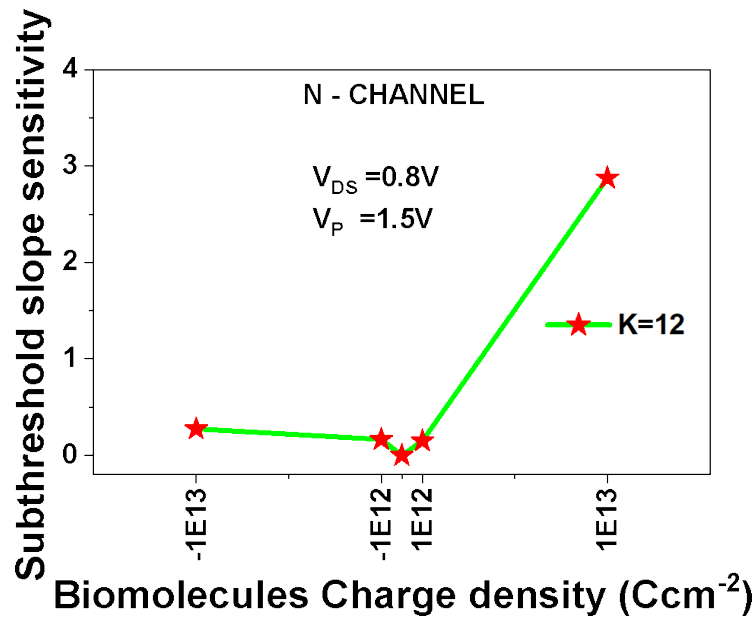


Fig 14(c): SS sensitivity analysis with varying charge density of charged bio-molecules for p-mode

The results are depicted in Figures 14c and 14d. With the escalation in charge density magnitude, there was a corresponding rise in SS sensitivity observed in both N-type and P-type modes. Specifically, in N-type mode, the highest SS sensitivity, reaching 2.87, was observed at $QF = 1E13 \text{ Ccm}^{-2}$.

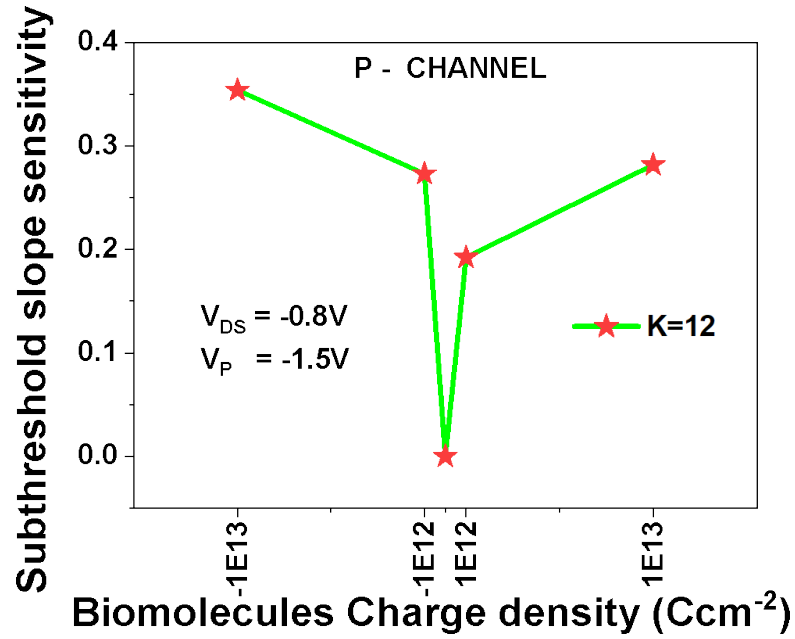


Fig 14(d): SS sensitivity analysis with varying charge density of charged biomolecules for p-mode

In contrast, within the P-type mode, the highest SS sensitivity was observed at $QF = -1E13 \text{ Ccm}^{-2}$, reaching a measurement of 0.35. Table 7 provides an illustration of the sensitivity of the proposed biosensor compared to the reported biosensor.

4.4.6 DC Output Parameters of UGC-RSiNW SBT Biosensor

A) N -Channel

TABLE5

S.NO	K	V _{th} (Volt)	SS (mV/dec)	I _{on}	I _{on} /I _{off}	QF
1	1	1.60	152	8.8 E-11	1.493 E9	0
2	2.63	1.48	91	7.14 E-9	2.06 E13	0
3	5	1.43	79	7.68 E-8	2.10 E13	0
4	12	0.83	36	2.46 E-7	1.26 E14	0
5	12	0.71	31	2.62 E-7	7.08 E13	1E12
6	12	1.03	142	6.60 E-7	2.39 E13	1E13
7	12	0.94	30	2.30 E-7	1.65 E15	-1E12
8	12	1.83	26	1.87 E-8	5.05 E12	-1E13

B) P- Channel

TABLE6

S.NO	K	V _t	SS (mV/dec)	I _{on}	I _{on} /I _{off}	Q _f (cm-2)
1	1	-1.70	116	2.64 E-10	1.28 E7	0
2	2.63	-1.71	85	6.42 E-9	3.25 E8	0
3	5	-1.67	77	3.63 E-8	2.78 E9	0
4	12	-1.62	72	2.55 E-7	1.34 E10	0
5	12	-1.70	86	1.76 E-7	7.61 E11	1E11
6	12	-1.77	93	1.02 E-12	73420.2	-1E11
7	12	-1.51	92	3.34 E-7	5.15 E12	1E12
8	12	-1.22	98	1.48 E-6	1.36 E11	-1E12

4.4.7 Sensitivity Comparison with the reported SiNW FET-based biosensors.

TABLE7

S.NO	QF	Vth Sensitivity
1	GAASiNanowireFET(K=12) [38]	0.157
2	NW_FET_Biosensor (K=10) [39]	0.07
3	C_RFET(N-type,K=12) [30]	0.01
4	C_RFET(P-type,K=12) [30]	0.05
5	VS-NW-FETBiosensor (K=10) [39]	0.14
6	ThisWork(N-typeK=12)	0.48
7	ThisWork(P-typeK=12)	0.04

CONCLUSION

This work delves into the performance capabilities of UGC-RSiNW SBT as a label-free biosensor, specifically focusing on its efficiency in detecting both neutral and charged bio-molecules. The proposed device demonstrates superior performance compared to traditional FET-based biosensors. For bio-molecules with neutral charges, the sensitivity in the n-mode for threshold voltage (V_{TH}) is significantly enhanced by 97.91%, whereas in the p-mode, the sensitivity sees an increase of 16% when compared to conventional RFET biosensors. This substantial improvement highlights the exceptional sensitivity of the proposed biosensor, making it highly effective for detecting neutral bio-molecules.

Moreover, the biosensor also shows remarkable sensitivity to charged bio-molecules. When examining positively charged bio-molecules, the biosensor exhibits a V_{TH} sensitivity of 0.24 (with a standard deviation of 0.09) in n-mode and an impressive 2.87 (with a standard deviation of 0.28) in p-mode. On the contrary, for negatively charged bio-molecules, the device displays a V_{TH} sensitivity of 1.2 (standard deviation 0.25) and a subthreshold swing (SS) sensitivity of 0.27 (standard deviation 0.35) for n-mode and p-mode, respectively. These observed sensitivities provide valuable insights into the performance characteristics of the biosensor, indicating its high potential for various biosensing applications.

The enhanced sensitivity of the UGC-RSiNW SBT biosensor to both neutral and charged bio-molecules underscores its versatility and robustness, making it an excellent candidate for a wide range of biosensing scenarios. This device not only meets but exceeds the sensitivity requirements for effective biomolecule detection, which is crucial for applications in medical diagnostics, environmental monitoring, and biochemical research. By offering high sensitivity and specificity, the proposed biosensor could pave the way for more accurate and reliable detection methods, ultimately contributing to advancements in the field of biosensing technology.

REFERENCES

- [1] Moore GE. Cramming more components onto integrated circuits, *Electronics* 1965, April 19; volume 38, number 8, pp.114.
- [2] Heinzig A, Slesazeck S, Kreupl F, Mikolajick T, Weber WM. Reconfigurable Silicon Nanowire Transistors. *Nano Lett.* 2012 Jan 11;12(1):119–24.
- [3] De Marchi M, Sacchetto D, Frache S, Zhang J, Gaillardon P, Leblebici Y, et al. Polarity control in double-gate, gate-all-around vertically stacked silicon nanowire FETs. *Electron Devices Meeting (IEDM)*, 2012; p. 8.4.1-8.4.4.
- [4] Lin Y-M, Appenzeller J, Knoch J, Avouris P. High-performance carbon nanotube field-effect transistor with tunable polarities. *IEEE Trans Nanotechnol.* 2005 Sep;4(5):481–9.
- [5] https://publik.tuwien.ac.at/files/publik_304335.pdf
- [6] <http://journal.auric.kr/jsts/XmlViewer/f383288>
- [7] <https://pubs.aip.org/aip/apr/article-abstract/10/1/011318/2881429/Band-to-band-tunneling-switches-based-on-two?redirectedFrom=fulltext>
- [8] Yang Cao, Guoliang Tian, Majumdar Sandip, Jinshun Bi, Kai Xi, Bo Li, "Numerical simulation of vertical tunnelling field-effect transistors charge-trapping memory with TCAD tools", *Semiconductor Science and Technology*, vol.36, no.4, pp.045013, 2021.
- [9] www.silvaco.com
- [10] Heinzig RA, Mikolajick T, Trommer J, Grimm D, Weber WM. Dually active silicon nanowire transistors and circuits with equal electron and hole transport. *Nano Lett* 2013;13(9):4176–81.
- [11] Lombardi C, Manzini S, Saporito A, Vanzi M. A physically based mobility model for numerical simulation of nonplanar devices. *IEEE Trans Comput-Aided Des Integr Circuits Syst* 1988;CAD-7(11):1164–71.
- [12] Granzner R, Polyakov VM, Schwierz F, Kittler M, Luyken RJ, Rösner W, et al. Simulation of nanoscale MOSFETs using modified drift-diffusion and hydrodynamic models and comparison with Monte Carlo results. *Microelectron Eng* 2006;83(2):241–6.
- [13] Arora ND, Hauser JR, Roulston DJ. Electron and hole mobilities in silicon as a function of concentration and temperature. *IEEE Trans Electron Devices* 1982;ED-29(2):292–5.

- [14] Chiang T-K. A new quasi-2-D threshold voltage model for short-channel junctionless cylindrical surrounding gate (JLCSG) MOSFETs. *IEEE Trans. Electron Devices* 2012;59(11):3127–9.
- [15] Saha Priyanka, Sarkhel Saheli, Sarkar Subir Kumar. Two-dimensional potential and threshold voltage modeling of work function engineered double gate high-k gate stack Schottky Barrier MOSFET. *J Electronic Mater*, Springer 2019;8(6):3823–32.
- [16] G. Hurkx, D. Klaassen, and M. Knuvers, “A new recombination model for device simulation including tunneling,” *IEEE Trans. Electron Devices*, vol. 39, no. 2, pp. 331–338, Feb. 1992
- [17] Lombardi C, Manzini S, Saporito A, Vanzi M. A physically based mobility model for numerical simulation of nonplanar devices. *IEEE Trans Comput-Aided Des Integr Circuits Syst* 1988;CAD-7(11):1164–71. <https://doi.org/10.1109/43.9186>.
- [18] D’Agostino F, Quercia D. Introduction to VLSI design (EECS 467), Short-Channel Effects in MOSFETs, December 11th (2000).
- [19] W.M.Weber, et al “Reconfigurable Nanowire electronics – A review”, *Solid-State Electronics*, ELSEVIER, 2014.
- [20] Bhattacharjee, A., & Dasgupta, S. (2017). Impact of Gate/Spacer-Channel Underlap, Gate Oxide EOT, and Scaling on the Device Characteristics of a DG-RFET. *IEEE Transactions on Electron Devices*, 64(8), 3063–3070. doi:10.1109/ted.2017.2710236
- [21] Poojari, N. N., Singh, R. R., Ahmed, N., Kale, S. (2022). A Comparative Study of Short Gate and Full Gate Dielectric Modulated Schottky Barrier TFET for Biosensing Application. *Silicon*, 14(18), 12223-12233.
- [22] Kumar, A., Kale, S. (2023). A Comparative Analysis of Cavity Positions in Charge Plasma based Tunnel FET for Biosensor Application. *IETE Journal of Research*, 1-14.
- [23] Kale, S., Kondekar, P. N. (2017). Design and investigation of dielectric engineered dopant segregated Schottky barrier MOSFET with NiSi source/drain. *IEEE Transactions on Electron Devices*, 64(11), 4400- 4407.
- [24] Kalra, S., Kumar, M. J., Dhawan, A. (2019). Reconfigurable FET biosensor for a wide detection range and electrostatically tunable sensing response. *IEEE Sensors Journal*, 20(5), 2261-2269.
- [25] Weber, W. M., Trommer, J., Grube, M., Heinzig, A., Konig, M., Mikolajick, T. (2014, March). Reconfigurable silicon nanowire devices and circuits: Opportunities and challenges. In *2014 Design, Automation & Test in Europe Conference & Exhibition (DATE)* (pp. 1-6). IEEE

- [26] Wu, P., Reis, D., Hu, X. S., Appenzeller, J. (2021). Two-dimensional transistors with reconfigurable polarities for secure circuits. *NATURE electronics*, 4(1), 45-53.
- [27] Bhattacharjee, A., Dasgupta, S. (2018). A compact physics-based surface potential and drain current model for an S/D spacer-based DG-RFET. *IEEE Transactions on Electron Devices*, 65(2), 448-455.
- [28] Biswas, A., Rajan, C., Samajdar, D. P. (2022). A Novel RFET Sensor for Label-Free Biomolecule Detection. *Silicon*, 14(15), 9533-9541.
- [29] Biswas, A., Rajan, C., Samajdar, D. P. (2022). A Novel HM-HD-RFET Biosensor for Label-Free Biomolecule Detection. *Journal of electronic materials*, 51(11), 6388-6396.
- [30] Saha, P., Dash, D. K., Sarkar, S. K. (2019). Nanowire reconfigurable FET as biosensor: Based on dielectric modulation approach. *Solid-State Electronics*, 161, 107637.
- [31] Kumar, A., Kale, S. (2023). Spacer-Engineered Reconfigurable Silicon Nanowire Schottky Barrier Transistor as a Label-Free Biosensor. *Silicon*, 1-14.
- [32] Heinzig, A., Slesazeck, S., Kreupl, F., Mikolajick, T., Weber, W. M. (2012). Reconfigurable silicon nanowire transistors. *Nano letters*, 12(1), 119-124.
- [33] SILVACO: Tcad device simulation software (2016), atlas, santa clara, ca, USA.
- [34] Kale, S., Latha, N. H., Bramhane, L. K. (2022). Design and Proposal of Double Pocket Schottky Barrier TFET with Dielectric Modulation for Biosensors Applications. *Silicon*, 14(16), 10957-10966.
- [35] Latha, N. H., Kale, S. (2020). Dielectric modulated Schottky barrier TFET for the application as label-free biosensor. *Silicon*, 12(11), 2673- 2679.
- [36] Singh, R., Kaim, S., MedhaShree, R., Kumar, A., Kale, S. (2022). Dielectric engineered Schottky barrier MOSFET for biosensor applications: proposal and investigation. *Silicon*, 14(8), 4053-4062.
- [37] Kale, S. (2023). Investigation of dual metal gate Schottky barrier MOSFET for suppression of ambipolar current. *IETE Journal of Research*, 69(1), 404-409.
- [38] Ashima, Dhandapani, V., Raj, B. (2023). Design and Performance Assessment of Graded Channel Gate-All-Around Silicon Nanowire FET for Biosensing Applications. *Silicon*, 15(8), 3535-3542.
- [39] Liu, F. C., Li, C., Guo, J. M., Jiang, H. F., You, H. L., Zhuang, Y. Q. (2020, November). A High Sensitivity Biosensor Based On Vertically Stacked Silicon Nanosheet-FET. In 2020 IEEE 15th international conference on solid-state and integrated circuit technology (ICSICT) (pp. 1-3). IEEE.

[40] Thakur, V., Kumar, A., Kale, S. (2024). Analytical modeling of spacer engineered reconfigurable silicon nanowire Schottky barrier transistor for biosensing applications. *Micro and Nanostructures*, 207799.

[41] A. Kumar, S. Kale, "Dual-k Reconfigurable Silicon Nanowire Schottky Barrier Transistor for Biosensing Application," presented at the 8th IEEE Electron Devices Technology and Manufacturing (EDTM) Conference, Bangalore, India, Mar. 3-6, 2024.

APPENDIX 1

CODE OF PROPOSED DEVICE

```
go atlas
tonyplot bhattacharjee.log
save outf=bhattacharjee.str
tonyplot3d bhattacharjee.str
##### VARIABLES #####
set LG=.100
#Radius
set R=.005
set TOX=.010
set dopingg_channel=1e15
set gatee_wfn=4.2
set source_wf=4.83
set drain_wf=4.83
set insula_permt=80
set LS=.010
set LD=.010
set LG1=0.040
set LG2=0.010
set LG3=0.040
set DE=0.020
set LCAVITY=0.025
set TE=0.010
set SIO2=0.001
#meshing
mesh cylindrical three.d
r.mesh l=0 spacing=0.005
r.mesh l=$R spacing=0.002
r.mesh l=$R+$SIO2 spacing=0.002
r.mesh l=$R+$TOX spacing=0.002
r.mesh l=$R+$TOX+$TE spacing=0.002
```

a.m l=0 spac=60
a.m l=360 spac=60
z.mesh l=0 spacing=0.005
z.mesh l=\$LS spacing=0.001
z.mesh l=\$LS+\$LGAP spacing=0.001
z.mesh l=\$LS+\$LGAP+\$LCAVITY spacing=0.005
z.mesh l=\$LS+\$LGAP+\$LG1 spacing=0.005
z.mesh l=\$LS+\$LGAP+\$LG1+\$LG2 spacing=0.005
z.mesh l=\$LS+\$LGAP+\$LG1+\$LG2+\$LG3 spacing=0.005
z.mesh l=\$LS+\$LGAP+\$LG1+\$LG2+\$LG3+\$LGAP spacing=0.001
z.mesh l=\$LS+\$LGAP+\$LG1+\$LG2+\$LG3+\$LGAP+\$LD spacing=0.005
region num=1 material=air a.min=0 a.max=360 z.min=0
z.max=\$LS+\$LGAP+\$LG1+\$LG2+\$LG3+\$LGAP+\$LD r.min=0
r.max=\$R+\$TOX+\$TE
region num=2 material=Silicon a.min=0 a.max=360 z.min=\$LS
z.max=\$LS+\$LGAP+\$LG1+\$LG2+\$LG3+\$LGAP r.min=0 r.max=\$R
region num=3 material=NiSi a.min=0 a.max=360 z.min=0.0 z.max=\$LS r.min=0
r.max=\$R
region num=4 material=NiSi a.min=0 a.max=360
z.min=\$LS+\$LGAP+\$LG1+\$LG2+\$LG3+\$LGAP
z.max=\$LS+\$LGAP+\$LG1+\$LG2+\$LG3+\$LGAP+\$LD r.min=0 r.max=\$R
region num=5 material=SiO2 a.min=0 a.max=360 z.min=\$LS+\$LGAP+\$LCAVITY
z.max=\$LS+\$LGAP+\$LCAVITY+\$LG1 r.min=\$R r.max=\$R+\$TOX
region num=6 material=SiO2 a.min=0 a.max=360 z.min=\$LS+\$LGAP+\$LG1
z.max=\$LS+\$LGAP+\$LG1+\$LG2 r.min=\$R r.max=\$R+\$TOX+\$TE
region num=7 material=TiO2 a.min=0 a.max=360 z.min=\$LS+\$LGAP+\$LG1+\$LG2
z.max=\$LS+\$LGAP+\$LG1+\$LG2+\$LG3 r.min=\$R r.max=\$R+\$TOX
region num=8 USER.material=DNA a.min=0 a.max=360 z.min=\$LS+\$LGAP
z.max=\$LS+\$LGAP+\$LCAVITY r.min=\$R+\$SIO2 r.max=\$R+\$TOX
region num=9 material=SIO2 a.min=0 a.max=360 z.min=\$LS+\$LGAP
z.max=\$LS+\$LGAP+\$LCAVITY r.min=\$R r.max=\$R+\$SIO2

#ELECTRODE

electrode name=source a.min=0 a.max=360 r.min=0 r.max=\$R z.min=0 z.max=\$LS

electrode name=drain a.min=0 a.max=360 r.min=0 r.max=\$R

z.min=\$LS+\$LGAP+\$LG1+\$LG2+\$LG3+\$LGAP-\$DE

z.max=\$LS+\$LGAP+\$LG1+\$LG2+\$LG3+\$LGAP+\$LD

electrode name=gate a.min=0 a.max=360 r.min=\$R+\$TOX r.max=\$R+\$TOX+\$TE

z.min=\$LS+\$LGAP z.max=\$LS+\$LGAP+\$LG1

electrode name=CATHODE a.min=0 a.max=360 r.min=\$R+\$TOX

r.max=\$R+\$TOX+\$TE z.min=\$LS+\$LGAP+\$LG1+\$LG2

z.max=\$LS+\$LGAP+\$LG1+\$LG2+\$LG3

doping region=2 uniform N.type conc=1e15

interface qf=0 a.min=0 a.max=360 z.min=\$LS+\$LGAP

z.max=\$LS+\$LGAP+\$LCAVITY r.min=\$R r.max=\$R+\$TOX

contact name=source WORKFUNC=\$source_wf nsurf.rec psurf.rec E.TUNNEL

H.TUNNEL barrier thermionic Me.tunnel=0.3 Mh.tunnel=0.2 alpha=1e-7

contact name=drain WORKFUNC=\$drain_wf nsurf.rec psurf.rec E.TUNNEL

H.TUNNEL barrier thermionic Me.tunnel=0.3 Mh.tunnel=0.2 alpha=1e-7

contact name=GATE workfunc=\$gate_wf

contact name=CATHODE workfunc=\$gate_wf

material material=Silicon affinity=4.17 EG300=1.12

#MATERIAL REGION=5 permittivity=\$insul_perm mc=0.0949 MV=0.5620

affinity=1.59 EG300=3.2

#MATERIAL REGION=6 permittivity=\$insul_perm mc=0.0949 MV=0.5620

affinity=1.59 EG300=3.2

#MATERIAL REGION=7 permittivity=\$insul_perm mc=0.0949 MV=0.5620

affinity=1.59 EG300=3.2

#####BIOMOLECULE#####

material material=DNA user.group=insulator user.default=oxide permittivity=5

#####MODELS#####

models AUGER UST BBT.NONLOCAL SRH CONMOB FLDMOB N.CONCAN

bqp.n evsatmod=0 BQP.QDIR = 3 print

models FERMI SRH BGN UST auger consrh ccsmob fldmob CVT bbt.std inject fnord

boltzman print temperature=300 BQP.QDIR = 4

```

models FERMI SRH BGN UST auger ccsmob CVT BBT.NONLOCAL fnord boltzman
print temperature=300 BQP.QDIR = 4
mobility bn.cvt=4.75e7 bp.cvt=9.925e6 cn.cvt=1.74e5 cp.cvt=8.842e5 taun.cvt=0.125
taup.cvt=0.0317 gamn.cvt=2.5 gamp.cvt=2.2 mu0n.cvt=52.2 mu0p.cvt=44.9
muln.cvt=43.4 mulp.cvt=29.0 mumaxn.cvt=1417.0 mumaxp.cvt=470.5
crn.cvt=9.68e16 crp.cvt=2.23e17 csncvt=3.43e20 csp.cvt=6.10e20 alphn.cvt=0.680
alphp.cvt=0.71 betan.cvt=2.0 betap.cvt=2.0 pcn.cvt=0.0 pcp.cvt=0.23e16
deln.cvt=5.82e14 delp.cvt=2.0546e14
method BICGST newton itlimit=25 limit print fix.qf trap atrap=0.5 maxtrap=6 autonr
nrcriterion=0.1 tol.time=5e-3 dt.min=1e-25
method carriers=2
##### Methods #####
method maxtrap=6 autonr nblokit=45 bicgst dvlimit=1.0 CARRIERS=2
output p.quantum band.temp con.band val.band band.par
solve init
#SOLVE VDRAIN=-0.14375 VCATHODE=-0.269531
SOLVE VDRAIN=0.4 VCATHODE=0.75
solve vdrain=0.8 vCATHODE=1.5
log outf=bhattacharjee.log
solve name=gate vgate=-2 vstep=0.2 vfinal=2
extract init inf="bhattacharjee.log"
extract name="vt1"(xintercept(maxslope(curve(v."gate",i."drain"))))
extract name="subvt"1.0/slope(maxslope(curve(abs(v."gate"),log10(abs(i."drain")))))
extract name="Ion"max(abs(i."drain"))
extract name="Ioff"min(abs(i."drain"))
extract name="Ion/Ioff"((max(abs(i."drain")))/(min(abs(i."drain"))))
extract name="gm"(slope(maxslope(curve(abs(v."gate"),abs(i."drain")))))
tonyplot bhattacharjee.log
save outf=bhattacharjee.str
tonyplot3d bhattacharjee.str
quit

```

PAPER NAME

plagfinal_dtu.pdf

AUTHOR

SURAJ YADAV

WORD COUNT

5218 Words

CHARACTER COUNT

28225 Characters

PAGE COUNT

35 Pages

FILE SIZE

3.2MB

SUBMISSION DATE

May 31, 2024 11:48 AM GMT+5:30

REPORT DATE

May 31, 2024 11:49 AM GMT+5:30

● 7% Overall Similarity

The combined total of all matches, including overlapping sources, for each database.

- 2% Internet database
- 5% Publications database
- Crossref database
- Crossref Posted Content database
- 3% Submitted Works database

● Excluded from Similarity Report

- Bibliographic material
- Cited material
- Small Matches (Less than 8 words)





2K22VLS21 SURAJKUMAR <surajkumar_2k22vls21@dtu.ac.in>

Decision on NANO 2024 submission 142

1 message

The PaperCept Conference/Journal Management System <nano@papercept.net>

Fri, May 17, 2024 at 5:34 PM

Reply-To: giovanni.finocchio@unime.it, gfinocchio@unime.it

To: sumitkale785@gmail.com

Cc: surajkumar_2k22vls21@dtu.ac.in, kaustubh@dtu.ac.in, anilkumar_2k20phdec13@dtu.ac.in

Message from The PaperCept Conference/Journal Management System

Message originated by Giovanni Finocchio

Dear Dr. Sumit Kale,

On behalf of the IEEE-Nano 2024 Technical Program Committee we are pleased to confirm the provisional acceptance of your paper (Id: 142):

Title: Sensitivity Investigation of Underlap Gate Cavity-Based Reconfigurable Silicon Nanowire Schottky Barrier Transistor for Biosensor Application

- for inclusion in the IEEE-NANO 2024 conference proceedings,
- for presentation at the IEEE-NANO 2024 conference,
- and for publication in IEEE Xplore

Note that the final submission deadline is June 5 - final date.

1. This provisional acceptance will become definitive only after we have received the following from you:

- a. camera-ready manuscript
- b. signed IEEE copyright form
- c. completed conference registration

Information for submission of the final manuscript and copies of the copyright form are available at <http://nano.papercept.net> which can be accessed from the IEEE-NANO 2024 website at: <https://2024.ieeenano.org>, where a guidance for final submission is also available. The submission site at <http://nano.papercept.net>.

2. Please note the following deadlines:

- a. Submission of the manuscript and copyright right forms: June 5
- b. Conference pre-registration discount rates: June 6

The presentation type will be sent on 1st June.

Thank you for your contribution to IEEE-NANO 2024 and on behalf of the Technical Program Committee we look forward to meeting you in Gijon, Spain in July.

Yours sincerely,

Program Chairs of the Conference

Giovanni Finocchio, University of Messina, Italy

Vito Puliafito, Politecnico di Bari, Italy

Jiayan Law, University of Sevilla, Spain

Conference chair Montserrat Rivas, University of Oviedo, Spain

Decision: Accepted as Contributed paper.

Submission information

Authors and title:

Suraj Kumar, Sumit Kale*, Kaustubh Ranjan Singh, Anil Kumar

Sensitivity Investigation of Underlap Gate Cavity-Based Reconfigurable Silicon Nanowire Schottky Barrier Transistor for Biosensor Application

Conference: 2024 IEEE 24th International Conference on Nanotechnology (NANO).

Current status: Accepted.

Submission number: 142.

To access your workspace please log in at <https://nano.papercept.net/conferences/scripts/start.pl> using your PIN 116905 and password

To see this decision message and the reviews (if any) choose the appropriate option under "Choose an option..." for this submission in your NANO 2024 author workspace

If you do not have your password then follow the link <https://nano.papercept.net/conferences/scripts/pinwizard.pl> to retrieve it

Prof. Giovanni Finocchio

Department of Mathematical and Computer Sciences, Physical Sciences and Earth Sciences

University of Messina, Messina, Italy

Viale F. Stagnmo D'Alcontres, 31

98166 Messina

Italy

E-mail address: giovanni.finocchio@unime.it, gfinocchio@unime.it

4 attachments

 **CommentsToAuthor.txt**
1K

 **Review1931.txt**
1K

 **Review1933.txt**
1K

 **iThenticateScanResult.txt**
2K